

# Robust linear domain decomposition schemes for reduced non-linear fracture flow models

Elyes Ahmed<sup>†</sup>    Alessio Fumagalli<sup>\*</sup>    Ana Budiša<sup>†</sup>    Eirik Keilegavlen<sup>†</sup>  
 Jan M. Nordbotten<sup>‡</sup>    Florin A. Radu<sup>†</sup>

December 16, 2024

## Abstract

In this work, we consider compressible single-phase flow problems in a porous media containing a fracture. In the latter, a non-linear pressure-velocity relation is prescribed. Using a non-overlapping domain decomposition procedure, we reformulate the global problem into a non-linear interface problem. We then introduce two new algorithms that are able to efficiently handle the non-linearity and the coupling between the fracture and the matrix, both based on linearization by the so-called L-scheme. The first algorithm, named MoLDD, uses the L-scheme to resolve the non-linearity, requiring at each iteration to solve the dimensional coupling via a domain decomposition approach. The second algorithm, called ItLDD, uses a sequential approach in which the dimensional coupling is part of the linearization iterations. For both algorithms, the computations are reduced only to the fracture by pre-computing, in an offline phase, a multiscale flux basis (the linear Robin-to-Neumann co-dimensional map), that represent the flux exchange between the fracture and the matrix. We present extensive theoretical findings and in particular, the stability and the convergence of both schemes are obtained, where user-given parameters are optimized to minimise the number of iterations. Examples on two important fracture models are computed with the library PorePy and agree with the developed theory.

**Key words:** Porous medium; reduced fracture models; generalized Forchheimer’s laws; mortar mixed finite element; multiscale flux basis; non-linear interface problem; non-overlapping domain decomposition; L-scheme.

## 1 Introduction

Fractures are ubiquitous in porous media and strongly affect the flow and transport. Several energy and environmental applications including carbon sequestration, geothermal energy, and ground-water contamination involve flow and transport problems in a porous medium containing fractures. Typically, fractures are thin and long formations that correspond to a fast pathway along which medium properties, such as permeability or porosity, differ from the adjacent formations (the rocks) (see [5, 19, 38, 43]). Since it appears to be the cornerstone of many complex fracture models, we consider here (on the fractures) non-Darcy flow generalized Forchheimer’s law [37].

### 1.1 Model problem

Let  $\Omega$  be a bounded domain in  $\mathbb{R}^d$ ,  $d \in \{2, 3\}$ , with boundary  $\Gamma := \partial\Omega$ . Furthermore, let  $T$  be the final time simulation and  $I := (0, T)$ . Suppose that  $\gamma \subset \Omega$  is a  $(d - 1)$ -dimensional surface that divides  $\Omega$  into

<sup>†</sup>Department of Mathematics, University of Bergen, P. O. Box 7800, N-5020 Bergen, Norway. elyes.ahmed@uib.no, ana.budisa@uib.no, eirik.keilegavlen@uib.no, jan.nordbotten@uib.no, florin.radu@uib.no,

<sup>\*</sup>Dipartimento di Scienze Matematiche, Politecnico di Torino, Corso Duca degli Abruzzi 24, 10129 Torino, Italy. alessio.fumagalli@polito.it,

<sup>‡</sup>Department of Civil and Environmental Engineering, Princeton University, Princeton, N. J., USA.

two subdomains:  $\Omega = \Omega_1 \cup \Omega_2 \cup \gamma$ , where  $\gamma := \partial\Omega_1 \cap \partial\Omega_2$  and  $\Gamma_i := \partial\Omega_i \cap \partial\Omega$ ,  $i \in \{1, 2\}$ . Assume that the flow in  $I \times \Omega_i$ ,  $i \in \{1, 2\}$ , is described by the system of equations

$$\mathbf{K}_i^{-1} \mathbf{u}_i + \nabla p_i = \mathbf{0} \quad \text{in } I \times \Omega_i, \quad (1.1a)$$

$$\partial_t p_i + \nabla \cdot \mathbf{u}_i = f_i \quad \text{in } I \times \Omega_i, \quad (1.1b)$$

$$p_i = 0 \quad \text{in } I \times \Gamma_i, \quad (1.1c)$$

$$p_i(\cdot, 0) = p_i^0 \quad \text{in } \Omega_i, \quad (1.1d)$$

and in  $I \times \gamma$ , by the following equations

$$\xi(\mathbf{u}_\gamma) + \mathbf{K}_\gamma^{-1} \mathbf{u}_\gamma + \nabla_\tau p_\gamma = \mathbf{0} \quad \text{in } I \times \gamma, \quad (1.2a)$$

$$\partial_t p_\gamma + \nabla_\tau \cdot \mathbf{u}_\gamma = f_\gamma + (\mathbf{u}_1 \cdot \mathbf{n}_1 + \mathbf{u}_2 \cdot \mathbf{n}_2) \quad \text{in } I \times \gamma, \quad (1.2b)$$

$$p_\gamma = 0 \quad \text{in } I \times \partial\gamma, \quad (1.2c)$$

$$p_\gamma(\cdot, 0) = p_\gamma^0 \quad \text{in } \gamma, \quad (1.2d)$$

where the transmission conditions

$$-\mathbf{u}_i \cdot \mathbf{n}_i + \alpha_\gamma p_i = \alpha_\gamma p_\gamma \quad \text{on } I \times \gamma, \quad (1.3)$$

for  $i \in \{1, 2\}$ , are prescribed. Here,  $\nabla_\tau$  denotes the  $(d-1)$ -dimensional gradient operator in the plane of  $\gamma$ ,  $\mathbf{K}_\gamma$  is the hydraulic conductivity tensor in the fracture,  $\mathbf{K}_i$  is the hydraulic conductivity tensor in the subdomain  $\Omega_i$  and  $\mathbf{n}_i$  is the outward unit normal vector to  $\partial\Omega_i$ ,  $i \in \{1, 2\}$ . The function  $\xi$  is a non-linear function extending the classical Forchheimer flow to more general laws. In (1.3), the coefficient  $\alpha_\gamma$  is proportional to the normal component of the permeability of the physical fracture and inversely proportional to the fracture width/aperture. The functions  $f_\gamma$  and  $f_i$ ,  $i \in \{1, 2\}$ , are source terms in the fracture and in the matrix, respectively. For simplicity we have imposed a homogeneous Dirichlet condition on the boundary  $\partial\Omega$ . Finally,  $p_\gamma^0$  and  $p_i^0$ ,  $i \in \{1, 2\}$ , are initial conditions.

The system (1.1)–(1.3) is a mixed-dimensional model for flow in fractured porous media: the equations (1.1b)–(1.1a) are the mass conservation equation and the Darcy's law equation in the subdomain  $\Omega_i$  while equations (1.2b)–(1.2a) are the lower-dimensional mass conservation and a non-Darcy flow generalized Forchheimer's law, in the fracture of co-dimension 1. Together, these equations form a non-standard transmission problem where the fracture system sees the surrounding matrix system through the source term  $(\mathbf{u}_1 \cdot \mathbf{n}_1 + \mathbf{u}_2 \cdot \mathbf{n}_2)$  in (1.2b), while the rock matrix system communicates to the fracture through Robin type boundary conditions (1.3). Note that the restriction to only one fracture is made for the ease of presentation, but the model and the analysis below can be extended straightforwardly to more fractures, see for example [1, 43].

## 1.2 Assumptions on the data and weak formulation

Let  $D \subseteq \Omega$ . For  $s \geq 0$ ,  $\|\cdot\|_{s,D}$  stands for the usual Sobolev norm on  $H^s(D)$ . If  $s = 0$ ,  $\|\cdot\|_D$  is simply the  $L^2$  norm and  $(\cdot, \cdot)_D$  stands for the  $L^2$  scalar product. We define the weak spaces in  $\Omega_i$  for  $i \in \{1, 2\}$  as

$$\mathbf{V}_i := \{\mathbf{v} \in \mathbf{H}(\text{div}, \Omega_i) : \mathbf{v} \cdot \mathbf{n}_i \in L^2(\gamma)\} \quad \text{and} \quad M_i := L^2(\Omega_i),$$

where we have implicitly considered the trace operator of  $\mathbf{v} \cdot \mathbf{n}_i$ . Moreover, we introduce their global versions by  $\mathbf{V} := \bigoplus_{i=1}^2 \mathbf{V}_i$  and  $M := \bigoplus_{i=1}^2 M_i$ . The mixed spaces on the fracture  $\gamma$ , are  $\mathbf{V}_\gamma := \mathbf{H}(\text{div}_\tau, \gamma)$  and  $M_\gamma := L^2(\gamma)$ . For simplicity of notation, we introduce the jump  $\llbracket \cdot \rrbracket$  given by  $\llbracket \mathbf{u} \cdot \mathbf{n} \rrbracket := \mathbf{u}_1 \cdot \mathbf{n}_1 + \mathbf{u}_2 \cdot \mathbf{n}_2$ . and the functions  $\mathbf{K}$  and  $f$  in  $\Omega_1 \cup \Omega_2$  such that  $\mathbf{K}_i := \mathbf{K}|_{\Omega_i}$ , and  $f_i := f|_{\Omega_i}$ ,  $i \in \{1, 2\}$ . Throughout the paper, we assume that the following assumptions hold true:

- (A1)  $\xi : \mathbb{R} \rightarrow \mathbb{R}$  is  $C^1$ , strictly increasing and Lipschitz continuous, i.e., there exist  $\xi_m > 0$  and  $L_\xi$  such that  $\xi_m \leq \xi'(\mathbf{u}) \leq L_\xi < \infty$ . Otherwise, we require bounded flux for the differential problem (1.1)–(1.3), i.e,  $\mathbf{u} \in [L^\infty(\Omega)]^d$ , when  $\xi$  is simply an increasing function ( $\xi' \geq 0$ ), and we let  $L_\xi := \sup_{|\mathbf{u}| \leq C_\xi} \xi'(\mathbf{u})$ , where  $C_\xi := \sup_{\mathbf{x} \in \bar{\Omega}} |\mathbf{u}(\mathbf{x})|$ .

- (A2)  $\mathbf{K} : \mathbb{R}^d \rightarrow \mathbb{R}^d$  is assumed to be constant in time and bounded; there exist  $c_{\mathbf{K}} > 0$  and  $C_{\mathbf{K}}$  such that  $\zeta^T \mathbf{K}^{-1}(\mathbf{x}) \zeta \geq c_{\mathbf{K}} |\zeta|^2$  and  $|\mathbf{K}^{-1}(\mathbf{x}) \zeta| \leq C_{\mathbf{K}} |\zeta|$  for a.e.  $\mathbf{x} \in \Omega_1 \cup \Omega_2$ ,  $\forall \zeta \in \mathbb{R}^d$ .
- (A3)  $\mathbf{K}_\gamma : \mathbb{R}^{d-1} \rightarrow \mathbb{R}^{d-1}$  is assumed to be constant in time and bounded; there exist  $c_{\mathbf{K},\gamma} > 0$  and  $C_{\mathbf{K},\gamma}$  such that  $\zeta^T \mathbf{K}_\gamma^{-1}(\mathbf{x}) \zeta \geq c_{\mathbf{K},\gamma} |\zeta|^2$  and  $|\mathbf{K}_\gamma^{-1}(\mathbf{x}) \zeta| \leq C_{\mathbf{K},\gamma} |\zeta|$  for a.e.  $\mathbf{x} \in \gamma$ ,  $\forall \zeta \in \mathbb{R}^{d-1}$ .
- (A4) The Robin parameter  $\alpha_\gamma$  is a strictly positive constant.
- (A5) The initial conditions are such that  $p_i^0 \in L^2(\Omega_i)$ ,  $i \in \{1, 2\}$ , and  $p_\gamma^0 \in L^2(\gamma)$ . The source terms are such that  $f_i \in L^2(0, T; L^2(\Omega_i))$ ,  $i \in \{1, 2\}$ , and  $f_\gamma \in L^2(0, T; L^2(\gamma))$ . For simplicity we further assume that  $f$  and  $f_\gamma$  are piecewise constant in time with respect to the temporal mesh introduced in Section 2.1.

**Remark 1.1 (On assumptions).** *The Lipschitz-continuity of  $\xi$  is not true when the function  $\xi$  (therefore the flux) is unbounded, as it is the case for generalized Forchheimer's law. However, for bounded flux  $\mathbf{u}$ , this can be verified. Otherwise, this assumption can be recovered by truncating the original function  $\xi$ . Obviously, the solution of the truncated problem will not in general solve the original one. See, for example [44].*

We introduce the bilinear forms  $a_i : \mathbf{V}_i \times \mathbf{V}_i \rightarrow \mathbb{R}$ ,  $b_i : \mathbf{V}_i \times M_i \rightarrow \mathbb{R}$  and  $c_i : M_i \times M_i \rightarrow \mathbb{R}$ ,  $i \in \{1, 2\}$ ,

$$a_i(\mathbf{u}, \mathbf{v}) := (\mathbf{K}^{-1} \mathbf{u}, \mathbf{v})_{\Omega_i} + \frac{1}{\alpha_\gamma} (\mathbf{u} \cdot \mathbf{n}_i, \mathbf{v} \cdot \mathbf{n}_i)_\gamma, \quad b_i(\mathbf{u}, q) := (\nabla \cdot \mathbf{u}, q)_{\Omega_i}, \quad c_i(p, q) := (p, q)_{\Omega_i}. \quad (1.4)$$

On the fracture, we define the bilinear forms  $a_\gamma : \mathbf{V}_\gamma \times \mathbf{V}_\gamma \rightarrow \mathbb{R}$ ,  $b_\gamma : \mathbf{V}_\gamma \times M_\gamma \rightarrow \mathbb{R}$  and  $c_\gamma : M_\gamma \times M_\gamma \rightarrow \mathbb{R}$ ,

$$a_\gamma(\mathbf{u}, \mathbf{v}) := (\mathbf{K}_\gamma^{-1} \mathbf{u}, \mathbf{v})_\gamma, \quad b_\gamma(\mathbf{u}, \mu) := (\nabla_\tau \cdot \mathbf{u}, \mu)_\gamma, \quad c_\gamma(\lambda, \mu) := (\lambda, \mu)_\gamma. \quad (1.5)$$

With the above notations, a weak solution of (1.1)–(1.3) is given in the following.

**Definition 1.2 (Mixed-dimensional weak solution).** *Assume that (A1)–(A5) hold true. We say that  $(\mathbf{u}, p) \in L^2(0, T; \mathbf{V}) \times H^1(0, T; M)$  and  $(\mathbf{u}_\gamma, p_\gamma) \in L^2(0, T; \mathbf{V}_\gamma) \times H^1(0, T; M_\gamma)$  form a weak solution of (1.1)–(1.3) if it satisfies, for each  $i \in \{1, 2\}$ ,*

$$a_i(\mathbf{u}, \mathbf{v}) - b_i(\mathbf{v}, p) + (p_\gamma, \mathbf{v} \cdot \mathbf{n}_i)_\gamma = 0 \quad \forall \mathbf{v} \in \mathbf{V}_i, \quad (1.6a)$$

$$c_i(\partial_t p, q) + b_i(\mathbf{u}, q) = (f, q)_{\Omega_i} \quad \forall q \in M_i, \quad (1.6b)$$

$$(\xi(\mathbf{u}_\gamma), \mathbf{v})_\gamma + a_\gamma(\mathbf{u}_\gamma, \mathbf{v}) - b_\gamma(\mathbf{v}, p_\gamma) = 0 \quad \forall \mathbf{v} \in \mathbf{V}_\gamma, \quad (1.6c)$$

$$c_\gamma(\partial_t p_\gamma, \mu) + b_\gamma(\mathbf{u}_\gamma, \mu) - (\llbracket \mathbf{u} \cdot \mathbf{n} \rrbracket, \mu)_\gamma = (f_\gamma, \mu)_\gamma \quad \forall \mu \in M_\gamma, \quad (1.6d)$$

together with the initial conditions (1.1d), and (1.2d) in a weak sense.

In this paper we assume that a weak solution by Definition 1.2 exists. For the static model, and when  $\xi$  stems from the classical the Forchheimer's law, the existence and uniqueness of a weak solution was shown in [38]. That of the linear case, i.e.,  $\xi := 0$ , was studied in [35]. Through the paper, we will also consider the case of continuous pressure across  $\gamma$  by letting  $\alpha_\gamma \rightarrow \infty$  in (1.3). For this case, we will use Definition 1.2 for the weak formulation keeping in mind that in (1.4)  $a_i$  is simply  $a_i(\mathbf{u}, \mathbf{v}) := (\mathbf{K}^{-1} \mathbf{u}, \mathbf{v})_{\Omega_i}$  and  $\mathbf{V}_i := \mathbf{H}(\text{div}, \Omega_i)$  for  $i \in \{1, 2\}$ .

### 1.3 Goal and positioning of the paper

The mixed-dimensional problem (1.1)–(1.3) is an alternative to the possibility to use fine grids of the spatial discretization in the (physical) fracture and thus reduces the computational cost. This idea was introduced in [5] for highly permeable fractures and in [6] for fractures that may be much more permeable than the surrounding medium or nearly impermeable [26, 29, 48]. Particularly, for “fast-path” fractures, Darcy's law is replaced by the classical Darcy-Forchheimer's law as established in [38]. We also refer to [3, 16, 39, 40, 54] for extensions to other flow models. Here, we extend the model in [1, 38] to unsteady non-Darcy flow generalized Forchheimer's law. The work can be extended straightforwardly to viscosity models for generalized Newtonian fluids, including the Power law, the Cross model and the Carreau model [24, 25].

Considerable research efforts have been conducted to mixed-dimensional fracture models. Several numerical schemes for steady models have been proposed, such as a cell-centered finite volume scheme in [34],

an extended finite element method in [21], a mimetic finite difference [8] and a block-centred finite difference method in [42]. We also mention several contributions on the application of mixed methods, on conforming and non-conforming grids [14, 20, 27, 43]; see [13] for detailed account of major contribution on fracture models and discretization approaches. The aforementioned numerical approaches solve coupled fracture-matrix models monolithically, which leads to a large system, particularly if mixed finite element (MFE) methods are adopted [42]. This is especially the case when incorporating different equations varied in type, such as coupling linear and non-linear systems, and where often interface conditions involve additional variables. Domain decomposition (DD) is an elegant tool for modeling such a multi-physics problem and can provide an effective tool for reducing computational complexity and performing parallel calculations. See [22, 47] for a general introduction of the subject. In [28], the authors combine domain decomposition techniques with mixed finite element methods for the reduced Darcy-Forchheimer fracture model (see [5, 35] for the linear case).

In this paper, we propose efficient DD methods to solve (1.6) combining the mortar mixed finite element method (MMFEM) [10, 32, 55] with non-overlapping domain decomposition [1, 5, 45] and the  $L$ -scheme method [41, 46]. Our method first reformulates (1.6) into an interface problem by eliminating the subdomain variables. The resulting problem posed only on the fracture is a *superposition* of a *non-linear local* flow operator within the fracture and a *linear non-local* one handling the flux contribution from the subdomains (Robin-to-Neumann type operator). After approximating this problem with the MMFEM in space and the backward Euler scheme in time, we obtain a non-linear system to solve at each time step. A first algorithm is then built with the  $L$ -scheme employed as a linearization procedure; a robust quasi-Newton method with a parameter  $L > 0$  mimicking the Jacobian from the Newton method [41, 46]. At each iteration of the  $L$ -scheme, an *inner iterative algorithm*, such as GMRes or any Krylov solver, is used to solve the linear interface problem [30]. The action of the interface operator requires solving subdomain problems with Robin boundary condition on the fracture. This algorithm referred to henceforth as the Monolithic LDD-scheme (MoLDD) is *Jacobian-free* and subdomain solves are done in parallel. This LDD scheme will be shown to be *unconditionally stable*. Stability and condition number estimates of the inner DD system are obtained as well as contraction estimates and rates of convergence for the outer scheme. While MoLDD offers an elegant outer-inner approach to solve the interface-fracture problem, there is a computational overhead associated with its non-local part (DD), see *e.g.* [1, 30]. Precisely, the dominant computational cost in this approach is measured by the number of subdomain solves; increasing the non-linearity or DD strength and refining the grids both lead to an increase in the number of iterations and the number of subdomain solves.

More recently, the  $L$ -scheme has gained attention as an efficient solver to treat simultaneously non-linear and coupling effects in complex problems. See for example [49] for an application of the  $L$ -scheme on a non-linear DD problem and [15] on a non-linear coupling one. Building further on this idea, we propose a second algorithm, in which the DD step is part of the linearization iterations (see [4, 17] for related works). In other words, the  $L$ -scheme is now synchronizing linearization and domain decomposition through one-loop algorithm. This approach referred as the Iterative LDD-scheme (ItLDD) differs from the one commonly used when dealing with non-linear interface problems in the context of DD [2, 12]. At each iteration it has the cost of the sequential approach, yet it converges to the fully monolithic approach. This approach reduces the computational costs as no inner DD solver is required and only a modest number of subdomain solves is required at each iteration, which still done in parallel. This algorithm increases *local to non-local cooperation* and saves time if one process is dominating the whole problem.

The second contribution of this paper concerns the robust and efficient implementation of the LDD schemes above. Precisely, the dominant computational costs in these schemes comes from the subdomain solves. To reduce this computational cost, we make use of the multiscale flux basis framework from [32]. The fact that the non-linearity in (1.6) is only within the local operator on the fracture, we can adopt the notion that the linear non-local contribution from the rock subdomains can be expressed as a superposition of multiscale basis functions [1, 31, 32]. These multiscale flux basis consists of the flux (or velocity trace) response from each fracture pressure degrees of freedom. They are computed by solving a *fixed* number of *steady* Robin subdomain problems, which is equal to the number of fracture pressure degrees of freedom per subdomain. An inexpensive linear combination of the multiscale flux basis functions then replaces the subdomain solves in any inner/outer iteration of the algorithms. This step of *freezing* the contributions on the flow from the rock matrices can be *easily coded*, *cheaply evaluated*, and *efficiently used* in *all the algorithms*. That is, it permits reusing the same basis functions to compare MoLDD with ItLDD as well as to simulate various linear and non-linear models for flow in the fracture by varying  $\xi$  and finally exploring

high and low permeable fractures. This is in total *conformity* with the spirit of *reduced basis* [11, 52, 53]. Crucially, if a fixed time step is used, our multiscale flux basis applied to a non-linear time-dependent problem are constructed only once in the offline phase. This should be kept in mind also for our numerical results reported in the last section. Numerical results are computed with the library PorePy [36].

## 1.4 Outline of the paper

This paper is organized as follows: Firstly, the approximation of problem (1.6) using the MMFEM in space and a backward Euler scheme in time is given in Section 2. Also, the reduction of this mixed-dimensional scheme into a non-linear interface one is introduced. The LDD-schemes are formulated in Section 3. In Section 4 and Section 5, the analysis of the schemes is presented. Section 6 describes the implementation based on the multiscale flux basis framework. Finally, we showcase the performance of our methods on several numerical examples in Section 7 and draw the conclusions in Section 8.

## 2 The DD formulation

As explained earlier, it is natural to solve the mixed-dimensional problem (1.6) using domain decomposition techniques, especially as these methods make it possible to take different time grids in the subdomains and in the fracture.

### 2.1 Discretisation in space and time

We introduce in this section the partitions of  $\Omega$  and  $(0, T)$ , basic notation, and the mortar mixed finite element discretization of the mixed-dimensional problem (1.6).

Let  $\mathcal{T}_{h,i}$  be a partition of the subdomain  $\Omega_i$  into either  $d$ -dimensional simplicial or rectangular elements. Moreover, we assume that these meshes are such that  $\mathcal{T}_h = \cup_{i=1}^2 \mathcal{T}_{h,i}$  forms a conforming finite element mesh on  $\Omega$ . We also let  $\mathcal{T}_{h,\gamma}$  be either a partition of the fracture  $\gamma$  induced by  $\mathcal{T}_h$  or slightly coarser. Denote  $h$  as the maximal mesh size of both  $\mathcal{T}_h$  and  $\mathcal{T}_{h,\gamma}$ .

For an integer  $N \geq 0$ , let  $(\tau^n)_{0 \leq n \leq N}$  denotes a sequence of positive real numbers corresponding to the discrete time steps such that  $T = \sum_{n=1}^N \tau^n$ . Let  $t^0 := 0$ , and  $t^n := \sum_{j=1}^n \tau^j$ ,  $1 \leq n \leq N$ , be the discrete times. Let  $I^n := (t^{n-1}, t^n]$ ,  $1 \leq n \leq N$ .

#### 2.1.1 Finite-dimensional spaces and projection operators

For the approximation of scalar unknowns, we introduce the approximation spaces  $M_h := M_{h,1} \times M_{h,2}$  and  $M_{h,\gamma}$ , where  $M_{h,i}$ ,  $i \in \{1, 2\}$ , and  $M_{h,\gamma}$  are the spaces of piecewise constant functions associated with  $\mathcal{T}_{h,i}$ ,  $i \in \{1, 2\}$  and  $\mathcal{T}_{h,\gamma}$ , respectively. For the vector unknowns, we introduce the approximation spaces  $\mathbf{V}_h := \mathbf{V}_{h,1} \times \mathbf{V}_{h,2}$  and  $\mathbf{V}_{h,\gamma}$ , where  $\mathbf{V}_{h,i}$ ,  $i \in \{1, 2\}$  and  $\mathbf{V}_{h,\gamma}$ , are the lowest-order Raviart-Thomas-Nédélec finite elements spaces associated with  $\mathcal{T}_{h,i}$ ,  $i \in \{1, 2\}$  and  $\mathcal{T}_{h,\gamma}$ , respectively. Thus,  $\mathbf{V}_h \times M_h \subset \mathbf{V} \times M$  and  $\mathbf{V}_{h,\gamma} \times M_{h,\gamma} \subset \mathbf{V}_\gamma \times M_\gamma$ . For all of the above spaces,

$$\nabla \cdot \mathbf{V}_h = M_h, \quad \text{and} \quad \nabla_\tau \cdot \mathbf{V}_{h,\gamma} = M_{h,\gamma}, \quad (2.1)$$

and there exists a projection  $\tilde{\Pi}_i : \mathbf{H}^{1/2+\epsilon}(\Omega_i) \cap \mathbf{V}_i \rightarrow \mathbf{V}_{h,i}$ ,  $i \in \{1, 2\}$ , (for any  $\epsilon > 0$ ) see *e.g.* [31], satisfying among other properties that for any  $\mathbf{u} \in \mathbf{H}^{1/2+\epsilon}(\Omega_i) \cap \mathbf{V}_i$

$$(\nabla \cdot (\mathbf{u} - \tilde{\Pi}_i \mathbf{u}), q)_{\Omega_i} = 0 \quad \forall q \in M_{h,i}, \quad (2.2)$$

$$((\mathbf{u} - \tilde{\Pi}_i \mathbf{u}) \cdot \mathbf{n}_i, \mathbf{v} \cdot \mathbf{n}_i)_{\partial\Omega_i} = 0 \quad \forall \mathbf{v} \in \mathbf{V}_{h,i}. \quad (2.3)$$

We also note that if  $\mathbf{u} \in \mathbf{H}^\epsilon(\Omega_i) \cap \mathbf{V}_i$ ,  $0 < \epsilon < 1$ ,  $\tilde{\Pi}_i \mathbf{u}$  is well-defined [51] and

$$\|\tilde{\Pi}_i \mathbf{u}\|_{\Omega_i} \lesssim \|\mathbf{u}\|_{\epsilon, \Omega_i} + \|\nabla \cdot \mathbf{u}\|_{\Omega_i}. \quad (2.4)$$

We introduce  $\mathcal{Q}_{h,i}$  the  $L^2$ -projection onto  $\mathbf{V}_{h,i} \cdot \mathbf{n}_i$  and denote  $\mathcal{Q}_{h,i}^T : \mathbf{V}_{h,i} \cdot \mathbf{n}_i \rightarrow M_{h,\gamma}$  as the  $L^2$ -projection from the normal velocity trace on the subdomains onto the mortar space  $M_{h,\gamma}$ . Thus, for all  $\lambda \in M_{h,\gamma}$  the condition

$$\|\lambda\|_\gamma \lesssim \|\mathcal{Q}_{h,1}\lambda\|_\gamma + \|\mathcal{Q}_{h,2}\lambda\|_\gamma, \quad (2.5)$$

can easily be verified if the mesh on the fracture  $\mathcal{T}_{h,\gamma}$  matches the one resulting from the surrounding subdomains, or if  $\mathcal{T}_{h,\gamma}$  is chosen slightly coarser [9, 14]. Note that (2.1) can be satisfied by choosing any of the usual MFE pairs. That of the condition (2.5) can be satisfied even if the space  $M_{h,\gamma}$  is (not much) richer than the space of normal traces on  $\gamma$  of elements of  $\mathbf{V}_h$  [31, 32].

### 2.1.2 The discrete scheme

The fully discrete scheme of the mixed-dimensional formulation (1.6) based on the MMFEM in space and the backward Euler scheme in time is defined through the following.

**Definition 2.1 (The mixed-dimensional scheme).** *At each time step  $n \geq 1$ , assuming  $(p_{h,\gamma}^{n-1}, p_h^{n-1})$  is given, we look for  $(\mathbf{u}_h^n, p_h^n) \in \mathbf{V}_h \times M_h$  and  $(\mathbf{u}_{h,\gamma}^n, p_{h,\gamma}^n) \in \mathbf{V}_{h,\gamma} \times M_{h,\gamma}$  such that, for  $i \in \{1, 2\}$ ,*

$$a_i(\mathbf{u}_h^n, \mathbf{v}) - b_i(\mathbf{v}, p_h^n) = -(p_{h,\gamma}^n, \mathbf{v} \cdot \mathbf{n}_i)_\gamma \quad \forall \mathbf{v} \in \mathbf{V}_h. \quad (2.6a)$$

$$c_i(p_h^n - p_h^{n-1}, q) + \tau^n b_i(\mathbf{u}_h^n, q) = \tau^n (f^n, \mu)_{\Omega_i} \quad \forall q \in M_h, \quad (2.6b)$$

$$(\xi(\mathbf{u}_{h,\gamma}^n), \mathbf{v}) + a_\gamma(\mathbf{u}_{h,\gamma}^n, \mathbf{v}) - b_\gamma(\mathbf{v}, p_{h,\gamma}^n) = 0 \quad \forall \mathbf{v} \in \mathbf{V}_{h,\gamma}, \quad (2.6c)$$

$$c_\gamma(p_{h,\gamma}^n - p_{h,\gamma}^{n-1}, \mu) + \tau^n b_\gamma(\mathbf{u}_{h,\gamma}^n, \mu) - \tau^n (\llbracket \mathbf{u}_h^n \cdot \mathbf{n} \rrbracket, \mu)_\gamma = \tau^n (f_\gamma^n, \mu)_\gamma \quad \forall \mu \in M_{h,\gamma}. \quad (2.6d)$$

## 2.2 Reduction into an interface problem

Following the algorithm in [1], we reduce the mixed-dimensional scheme in Definition 2.1 into a non-linear interface one posed on  $\gamma$ , which can be solved using an appropriate combination of a linearization method and an iterative Krylov solver. For  $i \in \{1, 2\}$ , we let

$$p_{h,i}^n = p_{h,i}^*(\lambda_{h,\gamma}^n) + \bar{p}_{h,i}^n \quad \text{and} \quad \mathbf{u}_{h,i}^n = \mathbf{u}_{h,i}^*(\lambda_{h,\gamma}^n) + \bar{\mathbf{u}}_{h,i}^n, \quad 1 \leq n \leq N, \quad (2.7)$$

where for  $\lambda_{h,\gamma}^n \in M_{h,\gamma}$ ,  $(\mathbf{u}_{h,i}^*(\lambda_{h,\gamma}^n), p_{h,i}^*(\lambda_{h,\gamma}^n)) \in \mathbf{V}_{h,i} \times M_{h,i}$  solves

$$a_i(\mathbf{u}_{h,i}^*(\lambda_{h,\gamma}^n), \mathbf{v}) - b_i(\mathbf{v}, p_{h,i}^*(\lambda_{h,\gamma}^n)) = -(\lambda_{h,\gamma}^n, \mathbf{v} \cdot \mathbf{n}_i)_\gamma \quad \forall \mathbf{v} \in \mathbf{V}_{h,i}, \quad (2.8a)$$

$$c_i(p_{h,i}^*(\lambda_{h,\gamma}^n), q) + \tau^n b_i(\mathbf{u}_{h,i}^*(\lambda_{h,\gamma}^n), q) = 0 \quad \forall q \in M_{h,i}, \quad (2.8b)$$

and  $(\bar{\mathbf{u}}_{h,i}^n, \bar{p}_{h,i}^n) \in \mathbf{V}_{h,i} \times M_{h,i}$  solves

$$a_i(\bar{\mathbf{u}}_{h,i}^n, \mathbf{v}) - b_i(\mathbf{v}, \bar{p}_{h,i}^n) = 0 \quad \forall \mathbf{v} \in \mathbf{V}_{h,i}, \quad (2.9a)$$

$$c_i(\bar{p}_{h,i}^n - p_{h,i}^{n-1}, q) + \tau^n b_i(\bar{\mathbf{u}}_{h,i}^n, q) = \tau^n (f^n, \mu)_{\Omega_i} \quad \forall q \in M_{h,i}, \quad (2.9b)$$

$$(\bar{p}_{h,i}^0, \mu)_{\Omega_i} = (p_{h,i}^0, \mu)_{\Omega_i} \quad \forall \mu \in M_{h,i}. \quad (2.9c)$$

Define the forms  $s_{\gamma,i} : M_{h,\gamma} \times M_{h,\gamma} \rightarrow \mathbb{R}$ ,  $i \in \{1, 2\}$ ,  $s_\gamma : M_{h,\gamma} \times M_{h,\gamma} \rightarrow \mathbb{R}$ , and  $g_\gamma^n : M_{h,\gamma} \rightarrow \mathbb{R}$ ,

$$s_{\gamma,i}(\lambda_{h,\gamma}^n, \mu) := (\mathcal{S}_{\gamma,i}^{\text{RtN}}(\lambda_{h,\gamma}^n), \mu)_\gamma := -(\mathbf{u}_{h,i}^*(\lambda_{h,\gamma}^n) \cdot \mathbf{n}_i, \mu)_\gamma, \quad (2.10a)$$

$$s_\gamma(\lambda_{h,\gamma}^n, \mu) := (\mathcal{S}_\gamma^{\text{RtN}}(\lambda_{h,\gamma}^n), \mu)_\gamma := \sum_{i=1}^2 s_{\gamma,i}(\lambda_{h,\gamma}^n, \mu), \quad (2.10b)$$

$$g_\gamma^n(\mu) := (g_\gamma^n, \mu)_\gamma := \sum_{i=1}^2 (\bar{\mathbf{u}}_{h,i}^n \cdot \mathbf{n}_i, \mu)_\gamma, \quad (2.10c)$$

where  $\mathcal{S}_{\gamma,i}^{\text{RtN}} : M_{h,\gamma} \rightarrow M_{h,\gamma}$ ,  $1 \leq i \leq 2$ , and  $\mathcal{S}_\gamma^{\text{RtN}} := \sum_{i=1}^2 \mathcal{S}_{\gamma,i}^{\text{RtN}}$  are Robin-to-Neumann type operators. Obviously, the operator  $\mathcal{S}_{\gamma,i}^{\text{RtN}}$  is linear. It is easy to verify that the non-linear mixed-dimensional scheme (2.6) is equivalent to the non-linear interface scheme.

**Definition 2.2 (The reduced scheme).** Given  $n \geq 1$  and  $\lambda_{h,\gamma}^{n-1}$ , find  $(\mathbf{u}_{h,\gamma}^n, \lambda_{h,\gamma}^n) \in \mathbf{V}_{h,\gamma} \times M_{h,\gamma}$  such that

$$(\xi(\mathbf{u}_{h,\gamma}^n, \mathbf{v}))_\gamma + a_\gamma(\mathbf{u}_{h,\gamma}^n, \mathbf{v}) - b_\gamma(\mathbf{v}, \lambda_{h,\gamma}^n) = 0 \quad \forall \mathbf{v} \in \mathbf{V}_{h,\gamma}, \quad (2.11a)$$

$$c_\gamma(\lambda_{h,\gamma}^n - \lambda_{h,\gamma}^{n-1}, \mu) + \tau^n b_\gamma(\mathbf{u}_{h,\gamma}^n, \mu) + \tau^n s_\gamma(\lambda_{h,\gamma}^n, \mu) = \tau^n (f_\gamma^n + g_\gamma^n, \mu)_\gamma \quad \forall \mu \in M_{h,\gamma}. \quad (2.11b)$$

In the next section, we propose two iterative approaches based on the  $L$ -scheme to solve (2.11). The first approach entails an inner-outer procedure of the form *linearize*  $\rightarrow$  *solve the DD*  $\rightarrow$  *update*, so that the  $L$ -scheme is used for the outer loop and the GMRes or any Krylov solver for the inner loop. The second approach is a one-loop procedure in which the  $L$ -scheme acts iteratively and simultaneously on the linearization and DD.

### 3 Robust L-type Domain-Decomposition (LDD) schemes

For the presentation of the algorithms, we shall denote the time step simply by  $\tau$ , keeping in mind it may depend on  $n$ .

#### 3.1 A monolithic LDD scheme

The monolithic LDD scheme (MoLDD) used to solve the interface problem (2.11) reads:

**Algorithm 3.1 (The MoLDD scheme).**

1. Give the initial data  $(\lambda_{h,\gamma}^0, p_h^0) \in M_{h,\gamma} \times M_h$ , the stabilization parameter  $L_\gamma > 0$  and the tolerance  $\epsilon > 0$ .
2. **Do**
  - (a) Increase  $n := n + 1$ .
  - (b) Choose an initial approximation  $\mathbf{u}_{h,\gamma}^{n,-1} \in \mathbf{V}_{h,\gamma}$  of  $\mathbf{u}_{h,\gamma}^n$ . Set  $k := -1$ .
  - (c) **Do**
    - i. Increase  $k := k + 1$ .
    - ii. Compute  $(\mathbf{u}_{h,\gamma}^{n,k}, \lambda_{h,\gamma}^{n,k}) \in \mathbf{V}_{h,\gamma} \times M_{h,\gamma}$  such that, for all  $(\mathbf{v}, \mu) \in \mathbf{V}_{h,\gamma} \times M_{h,\gamma}$ ,

$$(\xi(\mathbf{u}_{h,\gamma}^{n,k-1}) + L_\gamma(\mathbf{u}_{h,\gamma}^{n,k} - \mathbf{u}_{h,\gamma}^{n,k-1}), \mathbf{v})_\gamma + a_\gamma(\mathbf{u}_{h,\gamma}^{n,k}, \mathbf{v}) - b_\gamma(\mathbf{v}, \lambda_{h,\gamma}^{n,k}) = 0, \quad (3.1a)$$

$$c_\gamma(\lambda_{h,\gamma}^{n,k} - \lambda_{h,\gamma}^{n-1}, \mu) + \tau b_\gamma(\mathbf{u}_{h,\gamma}^{n,k}, \mu) + \tau s_\gamma(\lambda_{h,\gamma}^{n,k}, \mu) = \tau (f_\gamma^n + g_\gamma^n, \mu)_\gamma. \quad (3.1b)$$

$$\text{while } \frac{\|(\mathbf{u}_{h,\gamma}^{n,k}, \lambda_{h,\gamma}^{n,k}) - (\mathbf{u}_{h,\gamma}^{n,k-1}, \lambda_{h,\gamma}^{n,k-1})\|_\gamma}{\|(\mathbf{u}_{h,\gamma}^{n,k-1}, \lambda_{h,\gamma}^{n,k-1})\|_\gamma} \geq \epsilon.$$

- (d) Update the subdomain solutions via (2.7).

**while**  $n \leq N$ .

**Remark 3.2 (Advantages of MoLDD-scheme).** The advantages of Algorithm 3.1 are multiple: (i) the algorithm is Jacobian-free and independent of the initialization, (ii) subdomain solves can be done in parallel, (iii) we can reuse of existing  $d$ - and  $(d-1)$ -dimensional codes for solving linear Darcy problem, and (iv) optimal convergence rate is obtained with a stabilization amount determined efficiently through  $L_\gamma$ .

The MoLDD scheme involves the solution of a linear Darcy interface problem (3.1) at each iteration  $k \geq 0$ . To see that, we introduce the linear operators  $\mathbf{A}_{L,\gamma} : \mathbf{V}_{h,\gamma} \rightarrow \mathbf{V}_{h,\gamma}$  and  $\mathbf{B}_\gamma : \mathbf{V}_{h,\gamma} \rightarrow M_{h,\gamma}$ , defined as  $(\mathbf{A}_{L,\gamma} \mathbf{u}, \mathbf{v})_\gamma := a_\gamma(\mathbf{u}, \mathbf{v}) + L_\gamma(\mathbf{u}, \mathbf{v})_\gamma$ ,  $\forall \mathbf{u}, \mathbf{v} \in \mathbf{V}_{h,\gamma}$ , and  $(\mathbf{B}_\gamma \mathbf{u}, q) := b_\gamma(\mathbf{u}, q)$ ,  $\forall \mathbf{u} \in \mathbf{V}_{h,\gamma}$ ,  $\forall q \in M_{h,\gamma}$ . Now (3.1) becomes

$$\mathcal{A}_{\text{DD}} \begin{bmatrix} \mathbf{u}_{h,\gamma}^{n,k} \\ \lambda_{h,\gamma}^{n,k} \end{bmatrix} := \begin{bmatrix} \mathbf{A}_{L,\gamma} & \mathbf{B}_\gamma^\top \\ \mathbf{B}_\gamma & \mathcal{S}_\gamma^{\text{RtN}} + \mathbf{I}/\tau \end{bmatrix} \begin{bmatrix} \mathbf{u}_{h,\gamma}^{n,k} \\ \lambda_{h,\gamma}^{n,k} \end{bmatrix} = \begin{bmatrix} L_\gamma \mathbf{u}_{h,\gamma}^{n,k-1} - \xi(\mathbf{u}_{h,\gamma}^{n,k-1}) \\ g_\gamma^n + f_\gamma^n + \lambda_{h,\gamma}^{n-1}/\tau \end{bmatrix} := \mathcal{F}_\gamma, \quad (3.2)$$

which can be solved using a Krylov type method, such as GMRes or MINRes. Given an initial guess  $\mathbf{w}_{h,\gamma}^{(0)} = [\mathbf{u}_{h,\gamma}^{n,k,0}, \lambda_{h,\gamma}^{n,k,0}]^T$ , the GMRes algorithm generates a sequence of iterates  $\{\mathbf{w}_{h,\gamma}^{(m)}\}_{m \geq 1}$ , where  $\mathbf{w}_{h,\gamma}^{(m)}$  is a solution of the finite-dimensional minimization problem

$$\mathbf{w}_{h,\gamma}^{(m)} := \arg \min_{\Psi \in \mathbf{w}_{h,\gamma}^{(0)} + \mathcal{K}_m} \|\mathcal{F}_\gamma - \mathcal{A}_{\text{DD}} \Psi\|_\gamma, \quad (3.3)$$

as an approximate solution to (3.2), where  $\mathcal{K}_m$  is the  $m$ -th Krylov subspace generated by the initial residual  $\mathbf{r}_\gamma^{(0)} := \mathcal{F}_\gamma - \mathcal{A}_{\text{DD}} \mathbf{w}_{h,\gamma}^{(0)}$ , i.e.,

$$\mathcal{K}_m := \mathcal{K}_m(\mathcal{A}_{\text{DD}}, \mathbf{r}_\gamma^{(0)}) := \text{span}(\mathbf{r}_\gamma^{(0)}, \mathcal{A}_{\text{DD}} \mathbf{r}_\gamma^{(0)}, \dots, \mathcal{A}_{\text{DD}}^{m-1} \mathbf{r}_\gamma^{(0)}).$$

At each GMRes iteration  $m \geq 1$ , we need to evaluate the action of the Robin-to-Neumann type operator  $\mathcal{S}_\gamma^{\text{RtN}}$  via (2.10), representing physically the contributions on the flow from the subdomains by solving Robin subdomain problems (2.8). Therefore, the GMRes algorithm is implemented in the matrix-free context [1, 30, 32]. We summarize the evaluation of the interface operator by the following steps:

**Algorithm 3.3 (Evaluating the action of  $\mathcal{S}_\gamma^{\text{RtN}}$ ).**

1. Enter interface data  $\lambda_{h,\gamma}$ .
2. **For**  $i = 1 : 2$ 
  - (a) Project mortar pressure onto subdomain boundary, i.e.,  $\varphi_{h,\gamma,i} = \mathcal{Q}_{h,i}(\lambda_{h,\gamma})$ .
  - (b) Solve the subdomain problem (2.8) with Robin data  $\varphi_{h,\gamma,i}$ .
  - (c) Project the resulting flux onto the space  $M_{h,\gamma}$ , i.e.,  $\mathcal{S}_{\gamma,i}^{\text{RtN}}(\lambda_{h,\gamma}) = -\mathcal{Q}_{h,i}^T \mathbf{u}_{h,i}^*(\varphi_{h,\gamma,i}) \cdot \mathbf{n}_i$ .

**EndFor**

3. Compute the flow contribution from the subdomains to the fracture given by the flux jump across the fracture,

$$\mathcal{S}_\gamma^{\text{RtN}}(\lambda_{h,\gamma}) = \sum_{i \in \{1,2\}} \mathcal{S}_{\gamma,i}^{\text{RtN}}(\lambda_{h,\gamma}).$$

**Remark 3.4 (Computational cost).** The evaluation of  $\mathcal{S}_\gamma^{\text{RtN}}$  dominates the total computational costs in Algorithm 3.1 (step 2(b) of Algorithm 3.3). The number of subdomain solves required by this method at each time step  $n \geq 1$  is approximately equal to  $\sum_{k=1}^{N_{\text{Lin}}^n} N_{\text{DD}}^k$ , where  $N_{\text{Lin}}$  is the number of iterations of the  $L$ -scheme, and  $N_{\text{DD}}^k$  denotes the number of inner DD iterations. To set-up the right-hand side term  $f_\gamma^n$ , we need to solve once in the subdomains at each time step  $n \geq 1$ .

## 3.2 A robust iterative LDD-scheme

An alternative LDD-scheme to solve the interface problem (2.11) is to let the  $L$ -scheme act iteratively not only on the non-linearity as in Algorithm 3.1, but also on the fracture-matrix coupling. Additional stabilization term is then required for the inter-dimensional coupling. This iterative scheme reads:

**Algorithm 3.5 (The ItLDD scheme).**

1. Give  $(\lambda_{h,\gamma}^0, p_h^0) \in M_{h,\gamma} \times M_h$ , the stabilization parameters  $(L_{\gamma,p}, L_{\gamma,u}) > 0$ , and the tolerance  $\epsilon > 0$ .
2. **Do**
  - (a) Increase  $n := n + 1$ .
  - (b) Choose an initial approximation  $(\mathbf{u}_{h,\gamma}^{n,-1}, \lambda_{h,\gamma}^{n,-1}) \in \mathbf{V}_{h,\gamma} \times M_{h,\gamma}$  of  $(\mathbf{u}_{h,\gamma}^n, \lambda_{h,\gamma}^n)$ . Set  $k := -1$ .
  - (c) **Do**
    - i. Increase  $k := k + 1$ .
    - ii. Compute  $(\mathbf{u}_{h,\gamma}^{n,k}, \lambda_{h,\gamma}^{n,k}) \in \mathbf{V}_{h,\gamma} \times M_{h,\gamma}$  such that, for all  $(\mathbf{v}, \mu) \in \mathbf{V}_{h,\gamma} \times M_{h,\gamma}$ ,

$$(\xi(\mathbf{u}_{h,\gamma}^{n,k-1}) + L_{\gamma,u}(\mathbf{u}_{h,\gamma}^{n,k} - \mathbf{u}_{h,\gamma}^{n,k-1}), \mathbf{v})_\gamma + a_\gamma(\mathbf{u}_{h,\gamma}^{n,k}, \mathbf{v}) - b_\gamma(\mathbf{v}, \lambda_{h,\gamma}^{n,k}) = 0. \quad (3.4a)$$

$$c_\gamma(\lambda_{h,\gamma}^{n,k} - \lambda_{h,\gamma}^{n,k-1}, \mu) + \tau L_{\gamma,p}(\lambda_{h,\gamma}^{n,k} - \lambda_{h,\gamma}^{n,k-1}, \mu)_\gamma + \tau s_\gamma(\lambda_{h,\gamma}^{n,k-1}, \mu) + \tau b_\gamma(\mathbf{u}_{h,\gamma}^{n,k}, \mu) = \tau(f_\gamma^n + g_\gamma^n, \mu)_\gamma, \quad (3.4b)$$



While  $\frac{\|(\mathbf{u}_{h,\gamma}^{n,k}, \lambda_{h,\gamma}^{n,k}) - (\mathbf{u}_{h,\gamma}^{n,k-1}, \lambda_{h,\gamma}^{n,k-1})\|_\gamma}{\|(\mathbf{u}_{h,\gamma}^{n,k-1}, \lambda_{h,\gamma}^{n,k-1})\|_\gamma} \geq \epsilon$ .  
 (d) Update the subdomain solutions via (2.7).  
 while  $n \leq N$ .

**Remark 3.6 (Computational cost).** The linear problem (3.4) is solved with the GMRes iterations (3.3). It requires at each iteration  $k \geq 1$  only one solve per subdomain to evaluate the action of  $\mathcal{S}_\gamma^{\text{RtN}}$  via Algorithm 3.3 at the previous iteration, and this at each time step  $n \geq 1$ .

**Remark 3.7 (Advantages of ItLDD-scheme).** The advantages of the iterative approach described in Algorithm 3.5 are: (i) at each iteration  $k \geq 1$ , the systems in the fracture and the rock matrices cooperate sequentially in one loop and with negligible inter-processor communication, (ii) optimal convergence rate is obtained with precise stabilization parameters  $(L_{\gamma,p}, L_{\gamma,u})$ , (iii) subdomain solves can be done in parallel, and (iv) existing codes for  $d$ - and  $(d-1)$ -dimensional Darcy problems can be cheaply combined and used for practical simulations.

## 4 Analysis of MoLDD-scheme

The complete analysis of Algorithm 3.1 will be carried out in two steps: (i) we first study the stability of the iterate DD scheme (inner solver) and estimate the condition number, and (ii) we prove the convergence of the LDD scheme (outer solver), show the well-posedness of the discrete scheme, estimate the convergence rate and subsequently determine the optimal stabilization parameter. Throughout the paper, we will frequently use the standard identity

$$(a - b) \cdot a = \frac{1}{2} (a^2 - b^2 + (a - b)^2), \quad a, b \in \mathbb{R}, \quad (4.1)$$

and inequality

$$|ab| \leq \frac{1}{2\delta} a^2 + \frac{2}{\delta} b^2, \quad a, b, \delta \in \mathbb{R}, \delta > 0. \quad (4.2)$$

A key point in the analysis of the methods below are inverse inequalities.

**Lemma 4.1 (Inverse inequalities).** There exist positive constants  $C_{\text{dTr}}, C_{\text{inv}} > 0$  depending only on the shape regularity of the mesh such that

$$\|\mathbf{u}_h \cdot \mathbf{n}\|_{\partial\Omega_i} \leq C_{\text{dTr}} h^{-1/2} \|\mathbf{u}_h\|_{\Omega_i} \quad \forall \mathbf{u}_h \in \mathbf{V}_{h,i}, \quad (4.3)$$

$$\|\nabla_\tau \cdot \mathbf{u}_{h,\gamma}\|_\gamma \leq C_{\text{inv}} h^{-1} \|\mathbf{u}_{h,\gamma}\|_\gamma \quad \forall \mathbf{u}_{h,\gamma} \in \mathbf{V}_{h,\gamma}. \quad (4.4)$$

### 4.1 Analysis of the DD step

To simplify the analysis, we rewrite problem (3.1) as: find  $(\mathbf{u}_{h,\gamma}^{n,k}, \lambda_{h,\gamma}^{n,k}) \in \mathbf{V}_{h,\gamma} \times M_{h,\gamma}$  such that,

$$\mathcal{A}_\gamma((\mathbf{u}_{h,\gamma}^{n,k}, \lambda_{h,\gamma}^{n,k}), (\mathbf{v}, \mu)) + s_\gamma(\lambda_{h,\gamma}^{n,k}, \mu) = \mathcal{F}_\gamma^{n,k-1}(\mathbf{v}, \mu) \quad \forall (\mathbf{v}, \mu) \in \mathbf{V}_{h,\gamma} \times M_{h,\gamma}, \quad (4.5)$$

where

$$\mathcal{A}_\gamma((\mathbf{u}_{h,\gamma}, \lambda_{h,\gamma}), (\mathbf{v}, \mu)) := a_\gamma(\mathbf{u}_{h,\gamma}, \mathbf{v}) + L_\gamma(\mathbf{u}_{h,\gamma}, \mathbf{v})_\gamma + \frac{1}{\tau}(\lambda_{h,\gamma}, \mu)_\gamma + b_\gamma(\mathbf{u}_{h,\gamma}, \mu) - b_\gamma(\mathbf{v}, \lambda_{h,\gamma}), \quad (4.6a)$$

$$\mathcal{F}_\gamma^{n,k-1}(\mathbf{v}, \mu) := (\xi(\mathbf{u}_{h,\gamma}^{n,k-1}) + L_\gamma \mathbf{u}_{h,\gamma}^{n,k-1}, \mathbf{v})_\gamma + (f_\gamma^n + g_\gamma^n, \mu)_\gamma. \quad (4.6b)$$

Therein,  $\mathcal{A}_\gamma$  is the linearized flow system on the fracture and  $s_\gamma$  is the flow contribution from the rock matrices. The first result concerns the properties of the coupling term  $s_\gamma$ .

**Lemma 4.2 (Properties of the DD operator).** The interface bilinear form  $s_\gamma$  satisfies:

- $s_\gamma$  is symmetric positive and semi-definite on  $L^2(\gamma)$ .

- There exists a constant  $C_1 > 0$  independent of  $h$  such that, for all  $\lambda_{h,\gamma} \in M_{h,\gamma}$ ,

$$\left(C_1 \frac{C_{\mathbf{K}}}{\sqrt{c_{\mathbf{K}}}} + \frac{1}{\sqrt{\alpha_{\gamma}}}\right)^{-2} \|\lambda_{h,\gamma}\|_{\gamma}^2 \leq s_{\gamma}(\lambda_{h,\gamma}, \lambda_{h,\gamma}) \leq \alpha_{\gamma} \|\lambda_{h,\gamma}\|_{\gamma}^2. \quad (4.7)$$

*Proof.* Recalling (2.10), we take  $\mathbf{v} = \mathbf{u}_{h,i}^*(\mu)$  and  $q = p_{h,i}^*(\mu)$  in (2.8) to see that the bilinear form  $s_{\gamma}$  can be expressed as

$$s_{\gamma}(\lambda_{h,\gamma}, \mu) = \sum_{i=1}^2 \{a_i(\mathbf{u}_{h,i}^*(\lambda_{h,\gamma}), \mathbf{u}_{h,i}^*(\mu)) + c_i(p_{h,i}^*(\lambda_{h,\gamma}), p_{h,i}^*(\mu))\}. \quad (4.8)$$

It is now easy to see that the bilinear form  $s_{\gamma}$  is symmetric and positive semi-definite on  $L^2(\gamma)$ . We now show that if  $s_{\gamma}(\lambda_{h,\gamma}, \lambda_{h,\gamma}) = 0$ , then  $\lambda_{h,\gamma} = 0$  on  $M_{h,\gamma}$ . Note that  $s_{\gamma}(\lambda_{h,\gamma}, \lambda_{h,\gamma}) = 0$  implies that  $\mathbf{u}_{h,i}^*(\lambda_{h,\gamma}) = p_{h,i}^*(\lambda_{h,\gamma}) = 0$ . Again, (2.8) implies  $(\mathcal{Q}_{h,i}\lambda_{h,\gamma}, \mathbf{v} \cdot \mathbf{n}_i)_{\gamma} = (\lambda_{h,\gamma}, \mathbf{v} \cdot \mathbf{n}_i)_{\gamma} = 0$  for any  $\mathbf{v} \in \mathbf{V}_{h,i}$ . Thus, we can find some  $\mathbf{v}$  so that  $\mathbf{v} \cdot \mathbf{n}_i = \mathcal{Q}_{h,i}\lambda_{h,\gamma}$  and then  $\|\mathcal{Q}_{h,i}\lambda_{h,\gamma}\|_{\gamma} = 0$ . Finally, (2.5) shows that  $\lambda_{h,\gamma} = 0$  on  $\gamma$ .

We now infer the upper bound on  $s_{\gamma}$ . The assumption **(A2)** directly implies

$$c_{\mathbf{K}} \|\mathbf{u}_{h,i}\|_{\Omega_i}^2 + \frac{1}{\alpha_{\gamma}} \|\mathbf{u}_{h,i} \cdot \mathbf{n}_i\|_{\gamma}^2 \leq a_i(\mathbf{u}_{h,i}, \mathbf{u}_{h,i}), \quad \forall \mathbf{u}_{h,i} \in \mathbf{V}_{h,i}. \quad (4.9)$$

The definition (2.10) of  $s_{\gamma}$  gives

$$\begin{aligned} s_{\gamma}(\lambda_{h,\gamma}, \lambda_{h,\gamma}) &:= - \sum_{i=1}^2 (\lambda_{h,\gamma}, \mathbf{u}_{h,i}^*(\lambda_{h,\gamma}) \cdot \mathbf{n}_i)_{\gamma} \leq \sum_{i=1}^2 \|\mathbf{u}_{h,i}^*(\lambda_{h,\gamma}) \cdot \mathbf{n}_i\|_{\gamma} \|\lambda_{h,\gamma}\|_{\gamma} \\ &\leq \sum_{i=1}^2 \alpha_{\gamma}^{1/2} a_i(\mathbf{u}_{h,i}^*(\lambda_{h,\gamma}), \mathbf{u}_{h,i}^*(\lambda_{h,\gamma}))^{1/2} \|\lambda_{h,\gamma}\|_{\gamma}. \end{aligned} \quad (4.10)$$

This result together with (4.8) lead to the upper bound in (4.7). We prove the lower bound by induction. To this aim, we let  $(\psi_i, \mathbf{r}_i)$ ,  $i \in \{1, 2\}$ , be the solution of the auxiliary subdomain problem

$$\mathbf{r}_i + \mathbf{K}_i \nabla \psi_i = \mathbf{0}, \quad \text{in } \Omega_i, \quad (4.11a)$$

$$\nabla \cdot \mathbf{r}_i = 0, \quad \text{in } \Omega_i, \quad (4.11b)$$

$$\psi_i = 0, \quad \text{on } \Gamma_i, \quad (4.11c)$$

$$\mathbf{r}_i \cdot \mathbf{n}_i = \mathcal{Q}_{h,i}\lambda_{h,\gamma}, \quad \text{on } \gamma. \quad (4.11d)$$

For fracture network with immersed fractures or for subdomains with  $\Gamma_i = \emptyset$ ,  $\lambda_{h,\gamma}$  approximates the pressure on  $\gamma$ , which is determined up to a constant. This constant is fixed by a zero mean value constraint for  $M_{h,\gamma}$  [9, 27]. Thus, the auxiliary problem is well-posed since  $(\mathbf{r}_i \cdot \mathbf{n}_i, 1)_{\partial\Omega_i} = (\mathcal{Q}_{h,i}\lambda_{h,\gamma}, 1)_{\partial\Omega_i} = 0$ . Now, we choose  $\mathbf{v} = \tilde{\Pi}_i \mathbf{r}_i$  in (2.8), to obtain

$$\begin{aligned} \|\mathcal{Q}_{h,i}\lambda_{h,\gamma}\|_{\gamma}^2 &= (\lambda_{h,\gamma}, \tilde{\Pi}_i \mathbf{r}_i \cdot \mathbf{n}_i)_{\gamma} = -a_i(\mathbf{u}_{h,i}^*(\lambda_{h,\gamma}), \tilde{\Pi}_i \mathbf{r}_i) + b_i(\tilde{\Pi}_i \mathbf{r}_i, p_{h,i}^*(\lambda_{h,\gamma})) \\ &= -a_i(\mathbf{u}_{h,i}^*(\lambda_{h,\gamma}), \tilde{\Pi}_i \mathbf{r}_i) \leq CC_{\mathbf{K}} \|\mathbf{u}_{h,i}^*(\lambda_{h,\gamma})\|_{\Omega_i} \|\mathbf{r}_i\|_{1/2, \Omega_i} + \alpha_{\gamma}^{-1} \|\mathbf{u}_{h,i}^*(\lambda_{h,\gamma}) \cdot \mathbf{n}_i\|_{\gamma} \|\mathcal{Q}_{h,i}\lambda_{h,\gamma}\|_{\gamma} \\ &\leq (CC_{\mathbf{K}} \|\mathbf{u}_{h,i}^*(\lambda_{h,\gamma})\|_{\Omega_i} + \alpha_{\gamma}^{-1} \|\mathbf{u}_{h,i}^*(\lambda_{h,\gamma}) \cdot \mathbf{n}_i\|_{\gamma}) \|\mathcal{Q}_{h,i}\lambda_{h,\gamma}\|_{\gamma} \\ &\leq \left(C \frac{C_{\mathbf{K}}}{\sqrt{c_{\mathbf{K}}}} + \frac{1}{\sqrt{\alpha_{\gamma}}}\right) \sqrt{a_i(\mathbf{u}_{h,i}^*(\lambda_{h,\gamma}), \mathbf{u}_{h,i}^*(\lambda_{h,\gamma}))} \|\mathcal{Q}_{h,i}\lambda_{h,\gamma}\|_{\gamma}, \end{aligned} \quad (4.12)$$

where we used (4.9), assumption **(A2)** and the elliptic regularity (2.4) together with

$$\|\mathbf{r}_i\|_{1/2, \Omega_i} \lesssim \|\mathcal{Q}_{h,i}\lambda_{h,\gamma}\|_{\gamma}. \quad (4.13)$$

The bound (4.12) in combination with (4.8)-(4.9) and (2.5) delivers the lower bound in (4.7).  $\square$

As announced in the introduction, it is interesting to study the robustness of Algorithm 3.1 and Algorithm 3.5 for the limiting case in which the coefficient  $\alpha_\gamma \rightarrow \infty$  in the transmission conditions (1.3). This case is physically corresponding to a continuous pressure over the fracture interface.

**Lemma 4.3 (Parameter-robustness ( $\alpha_\gamma \rightarrow \infty$ )).** *In the case of continuous pressure across  $\gamma$ , there exists a constant  $C_2 > 0$  such that, for all  $\lambda_{h,\gamma} \in M_{h,\gamma}$ ,*

$$C_2 \frac{c_{\mathbf{K}}}{C_{\mathbf{K}}^2} \|\lambda_{h,\gamma}\|_\gamma^2 \leq s_\gamma(\lambda_{h,\gamma}, \lambda_{h,\gamma}) \leq \frac{C_{\text{dTr}}^2}{c_{\mathbf{K}}} h^{-1} \|\lambda_{h,\gamma}\|_\gamma^2. \quad (4.14)$$

*Proof.* Recalling the definition (2.10) of  $s_\gamma$ , we have

$$0 \leq s_\gamma(\lambda_{h,\gamma}, \lambda_{h,\gamma}) = - \sum_{i=1}^2 (\lambda_{h,\gamma}, \mathbf{u}_{h,i}^*(\lambda_{h,\gamma}) \cdot \mathbf{n}_i)_\gamma \leq \sum_{i=1}^2 \|\mathbf{u}_{h,i}^*(\lambda_{h,\gamma}) \cdot \mathbf{n}_i\|_\gamma \|\lambda_{h,\gamma}\|_\gamma, \quad (4.15)$$

$$\leq \sum_{i=1}^2 C_{\text{dTr}} h^{-1/2} \|\mathbf{u}_{h,i}(\lambda_{h,\gamma})\|_{\Omega_i} \|\lambda_{h,\gamma}\|_\gamma, \quad (4.16)$$

where in that case we used the discrete trace inequality (4.3). This result together with (4.8) and (4.9) leads to the upper bound in (4.14). By inspection of the proof of Lemma (4.2), starting as in (4.12) we promptly get the lower bound of (4.14).  $\square$

In the following, we denote by  $\|\cdot\|_{s,\gamma}$  the induced semi-norm from  $s_\gamma$  on  $L^2(\gamma)$ ,

$$\|\mu\|_{s,\gamma} := s_\gamma(\mu, \mu)^{1/2}, \quad \forall \mu \in L^2(\gamma). \quad (4.17)$$

We will also consider the following discrete norms:

$$\|(\mathbf{v}_{h,\gamma}, \mu_{h,\gamma})\|_{0,\tau,\star}^2 := \|\mathbf{K}_\gamma^{-\frac{1}{2}} \mathbf{v}_{h,\gamma}\|_\gamma^2 + \|L_\gamma^{\frac{1}{2}} \mathbf{v}_{h,\gamma}\|_\gamma^2 + \|\tau^{-\frac{1}{2}} \mu_{h,\gamma}\|_\gamma^2, \quad (4.18a)$$

$$\|\mathbf{v}_{h,\gamma}\|_{\mathbf{V}_{h,\gamma}}^2 := \|\mathbf{K}_\gamma^{-\frac{1}{2}} \mathbf{v}_{h,\gamma}\|_\gamma^2 + \|L_\gamma^{\frac{1}{2}} \mathbf{v}_{h,\gamma}\|_\gamma^2 + \|\tau^{\frac{1}{2}} \nabla_\tau \cdot \mathbf{v}_{h,\gamma}\|_\gamma^2, \quad (4.18b)$$

$$\|\mu_{h,\gamma}\|_{M_{h,\gamma}}^2 := \|\mu_{h,\gamma}\|_{s,\gamma}^2 + \|\tau^{-\frac{1}{2}} \mu_{h,\gamma}\|_\gamma^2, \quad (4.18c)$$

$$\|(\mathbf{v}_{h,\gamma}, \mu_{h,\gamma})\|_{1,\tau,\star}^2 := \|\mathbf{v}_{h,\gamma}\|_{\mathbf{V}_{h,\gamma}}^2 + \|\mu_{h,\gamma}\|_{M_{h,\gamma}}^2. \quad (4.18d)$$

We start with the estimate below.

**Lemma 4.4 (Inverse energy estimates).** *There holds for all  $(\mathbf{u}_{h,\gamma}, \lambda_{h,\gamma}) \in \mathbf{V}_{h,\gamma} \times M_{h,\gamma}$ ,*

$$\|(\mathbf{u}_{h,\gamma}, \lambda_{h,\gamma})\|_{1,\tau,\star} \leq \sqrt{\max((1 + C_{\text{inv}} c_{\mathbf{K},\gamma} \tau h^{-2}), (1 + \alpha_\gamma \tau))} \|(\mathbf{u}_{h,\gamma}, \lambda_{h,\gamma})\|_{0,\tau,\star}. \quad (4.19)$$

Furthermore, if  $1/\alpha_\gamma \rightarrow 0$ , there holds

$$\|(\mathbf{u}_{h,\gamma}, \lambda_{h,\gamma})\|_{1,\tau,\star} \leq \sqrt{\max((1 + C_{\text{inv}} c_{\mathbf{K},\gamma} \tau h^{-2}), (1 + C_{\text{dTr}}^2 c_{\mathbf{K}}^{-1} \tau h^{-1}))} \|(\mathbf{u}_{h,\gamma}, \lambda_{h,\gamma})\|_{0,\tau,\star}. \quad (4.20)$$

*Proof.* Owing to the inverse inequality (4.4), together with (4.7), we obtain (4.19), and if  $\alpha_\gamma \rightarrow \infty$ , we make use (4.14) to get (4.20).  $\square$

The following results are immediately verified.

**Lemma 4.5 (Boundedness on  $A_\gamma$ ).** *There holds for all  $(\mathbf{u}_{h,\gamma}, \lambda_{h,\gamma}), (\mathbf{v}_{h,\gamma}, \mu_{h,\gamma}) \in \mathbf{V}_{h,\gamma} \times M_{h,\gamma}$ ,*

$$\mathcal{A}_\gamma((\mathbf{u}_{h,\gamma}, \lambda_{h,\gamma}), (\mathbf{v}_{h,\gamma}, \mu_{h,\gamma})) \leq \|(\mathbf{u}_{h,\gamma}, \lambda_{h,\gamma})\|_{1,\tau,\star} \|(\mathbf{v}_{h,\gamma}, \mu_{h,\gamma})\|_{1,\tau,\star}. \quad (4.21)$$

**Lemma 4.6 (Positivity on  $A_\gamma$ ).** *There holds for all  $(\mathbf{u}_{h,\gamma}, \lambda_{h,\gamma}) \in \mathbf{V}_{h,\gamma} \times M_{h,\gamma}$ ,*

$$\mathcal{A}_\gamma((\mathbf{u}_{h,\gamma}, \lambda_{h,\gamma}), (\mathbf{u}_{h,\gamma}, \lambda_{h,\gamma})) = \|\mathbf{K}_\gamma^{-\frac{1}{2}} \mathbf{u}_{h,\gamma}\|_\gamma^2 + \|L_\gamma^{\frac{1}{2}} \mathbf{u}_{h,\gamma}\|_\gamma^2 + \|\tau^{-\frac{1}{2}} \lambda_{h,\gamma}\|_\gamma^2. \quad (4.22)$$

The above results are then used to prove the following stability estimate for  $A_\gamma + s_\gamma$ .

**Theorem 4.7 (Stability results).** *Let  $(\mathbf{u}_{h,\gamma}, \lambda_{h,\gamma}) \in \mathbf{V}_{h,\gamma} \times M_{h,\gamma}$ ,*

$$\frac{1}{6(1 + \tau\alpha_\gamma)^2} \|(\mathbf{u}_{h,\gamma}, \lambda_{h,\gamma})\|_{1,\tau,\star} \leq \sup_{(\mathbf{v}_{h,\gamma}, \mu_{h,\gamma}) \in \mathbf{V}_{h,\gamma} \times M_{h,\gamma}} \frac{\mathcal{A}_\gamma((\mathbf{u}_{h,\gamma}, \lambda_{h,\gamma}), (\mathbf{v}_{h,\gamma}, \mu_{h,\gamma})) + s_\gamma(\lambda_{h,\gamma}, \mu_{h,\gamma})}{\|(\mathbf{v}_{h,\gamma}, \mu_{h,\gamma})\|_{1,\tau,\star}}. \quad (4.23)$$

If  $\alpha_\gamma \rightarrow \infty$ , we have

$$\frac{1}{6(1 + C_{\text{dTr}}^2 c_{\mathbf{K}}^{-1} \frac{\tau}{h})^2} \|(\mathbf{u}_{h,\gamma}, \lambda_{h,\gamma})\|_{1,\tau,\star} \leq \sup_{(\mathbf{v}_{h,\gamma}, \mu_{h,\gamma}) \in \mathbf{V}_{h,\gamma} \times M_{h,\gamma}} \frac{\mathcal{A}_\gamma((\mathbf{u}_{h,\gamma}, \lambda_{h,\gamma}), (\mathbf{v}_{h,\gamma}, \mu_{h,\gamma})) + s_\gamma(\lambda_{h,\gamma}, \mu_{h,\gamma})}{\|(\mathbf{v}_{h,\gamma}, \mu_{h,\gamma})\|_{1,\tau,\star}}. \quad (4.24)$$

*Proof.* Let us first recall this inf-sup condition; given  $\lambda_{h,\gamma} \in M_{h,\gamma}$ , we construct an element  $\mathbf{r}_{h,\gamma} \in \mathbf{V}_{h,\gamma}$  such that

$$b_\gamma(\mathbf{r}_{h,\gamma}, \lambda_{h,\gamma}) = \|\lambda_{h,\gamma}\|_\gamma^2, \text{ and } \|\lambda_{h,\gamma}\|_\gamma \leq C(\gamma) \|\mathbf{r}_{h,\gamma}\|_\gamma. \quad (4.25)$$

Let  $\Psi_\gamma \in H_0^2(\gamma)$  be the solution of  $-\Delta_\tau \Psi_\gamma = \tau^{-1} \lambda_{h,\gamma}$ . Pose  $\mathbf{r}_\gamma = -\nabla_\tau \Psi_\gamma$  and let  $\mathbf{r}_{h,\gamma} = \Pi_{h,\gamma} \mathbf{r}_\gamma$ , where  $\Pi_{h,\gamma}$  is the Raviart-Thomas projection onto  $\mathbf{V}_{h,\gamma}$  [14, 38]. Then, we have  $\nabla_\tau \cdot \mathbf{r}_{h,\gamma} = \Pi_{h,\gamma} \nabla_\tau \cdot \mathbf{r}_\gamma = \tau^{-1} \lambda_{h,\gamma}$ . Hence,  $b_\gamma(\mathbf{r}_{h,\gamma}, \lambda_{h,\gamma}) = \|\tau^{-\frac{1}{2}} \lambda_{h,\gamma}\|_\gamma^2$ . Furthermore, we have  $\|\mathbf{r}_{h,\gamma}\|_\gamma^2 = \|\Pi_{h,\gamma} \mathbf{r}_\gamma\|_\gamma^2 \leq C \|\mathbf{r}_\gamma\|_{1,\gamma}^2 = C \|\nabla_\tau \Psi_\gamma\|_{1,\gamma}^2 \leq C \|\Psi_\gamma\|_{2,\gamma}^2 \leq C(\gamma) \|\tau^{-\frac{1}{2}} \lambda_{h,\gamma}\|_\gamma^2$ .

Now, consider  $\delta_1, \delta_2 > 0$ , and let  $\mathbf{v}_{h,\gamma} = \mathbf{u}_{h,\gamma} - \delta_2 \mathbf{r}_{h,\gamma}$  and  $\mu_{h,\gamma} = \lambda_{h,\gamma} + \delta_1 \tau \nabla_\tau \cdot \mathbf{u}_{h,\gamma}$ , where  $\mathbf{r}_{h,\gamma}$  is from (4.25). We have

$$\begin{aligned} \mathcal{A}_\gamma((\mathbf{u}_{h,\gamma}, \lambda_{h,\gamma}), (\mathbf{v}_{h,\gamma}, \mu_{h,\gamma})) + s_\gamma(\lambda_{h,\gamma}, \mu_{h,\gamma}) &= \{\mathcal{A}_\gamma((\mathbf{u}_{h,\gamma}, \lambda_{h,\gamma}), (\mathbf{u}_{h,\gamma}, \lambda_{h,\gamma})) + s_\gamma(\lambda_{h,\gamma}, \lambda_{h,\gamma})\} \\ &\quad + \delta_1 \{\mathcal{A}_\gamma((\mathbf{u}_{h,\gamma}, \lambda_{h,\gamma}), \tau(\mathbf{0}, \nabla_\tau \cdot \mathbf{u}_{h,\gamma})) + s_\gamma(\lambda_{h,\gamma}, \tau \nabla_\tau \cdot \mathbf{u}_{h,\gamma})\} \\ &\quad - \delta_2 \{\mathcal{A}_\gamma((\mathbf{u}_{h,\gamma}, \lambda_{h,\gamma}), (\mathbf{r}_{h,\gamma}, 0))\}. \end{aligned} \quad (4.26)$$

For the first term on the right-hand side of (4.26), we obtain using estimate (4.22) together with (4.17),

$$\mathcal{A}_\gamma((\mathbf{u}_{h,\gamma}, \lambda_{h,\gamma}), (\mathbf{u}_{h,\gamma}, \lambda_{h,\gamma})) + s_\gamma(\lambda_{h,\gamma}, \lambda_{h,\gamma}) = \|\mathbf{K}_\gamma^{-\frac{1}{2}} \mathbf{u}_{h,\gamma}\|_\gamma^2 + \|L_\gamma^{\frac{1}{2}} \mathbf{u}_{h,\gamma}\|_\gamma^2 + \|\tau^{-\frac{1}{2}} \lambda_{h,\gamma}\|_\gamma^2 + \|\lambda_{h,\gamma}\|_{s,\gamma}^2.$$

For the second term, we get for all  $\epsilon_1 > 0$ ,

$$\begin{aligned} &\{\mathcal{A}_\gamma((\mathbf{u}_{h,\gamma}, \lambda_{h,\gamma}), \tau(\mathbf{0}, \nabla_\tau \cdot \mathbf{u}_{h,\gamma})) + s_\gamma(\lambda_{h,\gamma}, \tau \nabla_\tau \cdot \mathbf{u}_{h,\gamma})\} \\ &= \|\tau^{\frac{1}{2}} \nabla_\tau \cdot \mathbf{u}_{h,\gamma}\|_\gamma^2 + (\lambda_{h,\gamma}, \nabla_\tau \cdot \mathbf{u}_{h,\gamma})_\gamma + s_\gamma(\lambda_{h,\gamma}, \tau \nabla_\tau \cdot \mathbf{u}_{h,\gamma}) \\ &\geq \|\tau^{\frac{1}{2}} \nabla_\tau \cdot \mathbf{u}_{h,\gamma}\|_\gamma^2 - \|\tau^{\frac{1}{2}} \nabla_\tau \cdot \mathbf{u}_{h,\gamma}\|_\gamma \|\tau^{-\frac{1}{2}} \lambda_{h,\gamma}\|_\gamma - \alpha_\gamma \tau \|\tau^{\frac{1}{2}} \nabla_\tau \cdot \mathbf{u}_{h,\gamma}\|_\gamma \|\tau^{-\frac{1}{2}} \lambda_{h,\gamma}\|_\gamma \\ &\geq (1 - \epsilon_1 \frac{(1 + \tau\alpha_\gamma)}{2}) \|\tau^{\frac{1}{2}} \nabla_\tau \cdot \mathbf{u}_{h,\gamma}\|_\gamma^2 - \frac{(1 + \tau\alpha_\gamma)}{2\epsilon_1} \|\tau^{-\frac{1}{2}} \lambda_{h,\gamma}\|_\gamma^2. \end{aligned} \quad (4.27)$$

where we have used the continuity of  $s_\gamma$ , i.e.,

$$s_\gamma(\lambda_{h,\gamma}, \mu_{h,\gamma}) \leq \|\lambda_{h,\gamma}\|_{s,\gamma} \|\mu_{h,\gamma}\|_{s,\gamma} \leq \alpha_\gamma \|\lambda_{h,\gamma}\|_\gamma \|\mu_{h,\gamma}\|_\gamma. \quad (4.28)$$

For the last term, using (A2) together with (4.25) (first equation), we obtain for all  $\epsilon_2 > 0$ ,

$$\begin{aligned} \mathcal{A}_\gamma((\mathbf{u}_{h,\gamma}, \lambda_{h,\gamma}), (\mathbf{r}_{h,\gamma}, 0)) &\leq \frac{1}{2\epsilon_2} (\|\mathbf{K}_\gamma^{-\frac{1}{2}} \mathbf{u}_{h,\gamma}\|_\gamma^2 + \|L_\gamma^{\frac{1}{2}} \mathbf{u}_{h,\gamma}\|_\gamma^2) + \frac{\epsilon_2}{2} (\|\mathbf{K}_\gamma^{-\frac{1}{2}} \mathbf{r}_{h,\gamma}\|_\gamma^2 + \|L_\gamma^{\frac{1}{2}} \mathbf{r}_{h,\gamma}\|_\gamma^2) - b_\gamma(\mathbf{r}_{h,\gamma}, \lambda_{h,\gamma}) \\ &= \frac{1}{2\epsilon_2} (\|\mathbf{K}_\gamma^{-\frac{1}{2}} \mathbf{u}_{h,\gamma}\|_\gamma^2 + \|L_\gamma^{\frac{1}{2}} \mathbf{u}_{h,\gamma}\|_\gamma^2) + \frac{\epsilon_2}{2} (\|\mathbf{K}_\gamma^{-\frac{1}{2}} \mathbf{r}_{h,\gamma}\|_\gamma^2 + \|L_\gamma^{\frac{1}{2}} \mathbf{r}_{h,\gamma}\|_\gamma^2) - \|\tau^{-\frac{1}{2}} \lambda_{h,\gamma}\|_\gamma^2 \\ &\leq \frac{1}{2\epsilon_2} (\|\mathbf{K}_\gamma^{-\frac{1}{2}} \mathbf{u}_{h,\gamma}\|_\gamma^2 + \|L_\gamma^{\frac{1}{2}} \mathbf{u}_{h,\gamma}\|_\gamma^2) + \frac{\epsilon_2}{2} (C_{\mathbf{K},\gamma} + L_\gamma) C(\gamma) \|\mathbf{r}_{h,\gamma}\|_\gamma^2 - \|\tau^{-\frac{1}{2}} \lambda_{h,\gamma}\|_\gamma^2. \end{aligned} \quad (4.29)$$

Thus, with (4.25) (second equation),

$$-\delta_2 \mathcal{A}_\gamma((\mathbf{u}_{h,\gamma}, \lambda_{h,\gamma}), (\mathbf{r}_{h,\gamma}, 0)) \geq \delta_2 \left( 1 - \epsilon_2 \frac{C(\gamma)(C_{\mathbf{K},\gamma} + L_\gamma)}{2} \right) \|\tau^{-\frac{1}{2}} \lambda_{h,\gamma}\|_\gamma^2 - \frac{\delta_2}{2\epsilon_2} (\|\mathbf{K}_\gamma^{-\frac{1}{2}} \mathbf{u}_{h,\gamma}\|_\gamma^2 + \|L_\gamma^{\frac{1}{2}} \mathbf{u}_{h,\gamma}\|_\gamma^2). \quad (4.30)$$

Collecting the previous results we get

$$\begin{aligned} & \mathcal{A}_\gamma((\mathbf{u}_{h,\gamma}, \lambda_{h,\gamma}), (\mathbf{v}_{h,\gamma}, \mu_{h,\gamma})) + s_\gamma(\lambda_{h,\gamma}, \mu_{h,\gamma}) \\ & \geq \left( 1 - \frac{\delta_2}{2\epsilon_2} \right) (\|\mathbf{K}_\gamma^{-\frac{1}{2}} \mathbf{u}_{h,\gamma}\|_\gamma^2 + \|L_\gamma^{\frac{1}{2}} \mathbf{u}_{h,\gamma}\|_\gamma^2) + \delta_1 \left( 1 - \epsilon_1 \frac{(1 + \tau\alpha_\gamma)}{2} \right) \|\tau^{\frac{1}{2}} \nabla_\tau \cdot \mathbf{u}_{h,\gamma}\|_\gamma^2 \\ & \quad + \left( 1 - \delta_1 \frac{(1 + \tau\alpha_\gamma)}{2\epsilon_1} \right) \|\tau^{-\frac{1}{2}} \lambda_{h,\gamma}\|_\gamma^2 + \|\lambda_{h,\gamma}\|_{s,\gamma}^2 + \delta_2 \left( 1 - \epsilon_2 \frac{C(\gamma)(C_{\mathbf{K},\gamma} + L_\gamma)}{2} \right) \|\tau^{-\frac{1}{2}} \lambda_{h,\gamma}\|_\gamma^2. \end{aligned} \quad (4.31)$$

Now, let us choose the parameters  $\epsilon_i$  and  $\delta_i$  such that all the norms in (4.31) are multiplied by positive coefficients. We choose  $\epsilon_1 = 1/(1 + \tau\alpha_\gamma)$  and  $\delta_1 = 1/(1 + \tau\alpha_\gamma)^2$ , and then  $\epsilon_2 = 2/[C(\gamma)(C_{\mathbf{K},\gamma} + L_\gamma)]$  and  $\delta_2 = 2/[C(\gamma)(C_{\mathbf{K},\gamma} + L_\gamma) + 1]$ , to get

$$\begin{aligned} & \mathcal{A}_\gamma((\mathbf{u}_{h,\gamma}, \lambda_{h,\gamma}), (\mathbf{v}_{h,\gamma}, \mu_{h,\gamma})) + s_\gamma(\lambda_{h,\gamma}, \mu_{h,\gamma}) \\ & \geq \frac{C(\gamma)(C_{\mathbf{K},\gamma} + L_\gamma) + 2}{2(C(\gamma)(C_{\mathbf{K},\gamma} + L_\gamma) + 1)} (\|\mathbf{K}_\gamma^{-\frac{1}{2}} \mathbf{u}_{h,\gamma}\|_\gamma^2 + \|L_\gamma^{\frac{1}{2}} \mathbf{u}_{h,\gamma}\|_\gamma^2) + \frac{1}{2(1 + \tau\alpha_\gamma)^2} \|\tau^{\frac{1}{2}} \nabla_\tau \cdot \mathbf{u}_{h,\gamma}\|_\gamma^2 \\ & \quad + \frac{1}{2} \|\tau^{-\frac{1}{2}} \lambda_{h,\gamma}\|_\gamma^2 + \|\lambda_{h,\gamma}\|_{s,\gamma}^2. \end{aligned} \quad (4.32)$$

Thus,

$$\mathcal{A}_\gamma((\mathbf{u}_{h,\gamma}, \lambda_{h,\gamma}), (\mathbf{v}_{h,\gamma}, \mu_{h,\gamma})) + s_\gamma(\lambda_{h,\gamma}, \mu_{h,\gamma}) \geq \frac{1}{2(1 + \tau\alpha_\gamma)^2} \|(\mathbf{u}_{h,\gamma}, \lambda_{h,\gamma})\|_{1,\tau,\star}^2. \quad (4.33)$$

We also have

$$\begin{aligned} \|(\mathbf{v}_{h,\gamma}, \mu_{h,\gamma})\|_{1,\tau,\star} &= \|(\mathbf{u}_{h,\gamma} - \delta_2 \mathbf{r}_{h,\gamma}, \lambda_{h,\gamma} + \delta_1 \tau \nabla_\tau \cdot \mathbf{u}_{h,\gamma})\|_{1,\tau,\star} \\ &\leq \|(\mathbf{u}_{h,\gamma}, \lambda_{h,\gamma})\|_{1,\tau,\star} + \delta_1 \|(\mathbf{0}, \tau \nabla_\tau \cdot \mathbf{u}_{h,\gamma})\|_{1,\tau,\star} + \delta_2 \|(\mathbf{r}_{h,\gamma}, 0)\|_{1,\tau,\star}. \end{aligned}$$

With simple calculations, it is inferred that

$$\delta_1 \|(\mathbf{0}, \tau \nabla_\tau \cdot \mathbf{u}_{h,\gamma})\|_{1,\tau,\star} \leq \frac{1}{(1 + \tau\alpha_\gamma)^{\frac{3}{2}}} \|(\mathbf{u}_{h,\gamma}, \lambda_{h,\gamma})\|_{1,\tau,\star}, \quad (4.34a)$$

$$\delta_2 \|(\mathbf{r}_{h,\gamma}, 0)\|_{1,\tau,\star} \leq \frac{2\sqrt{C(\gamma)(C_{\mathbf{K},\gamma} + L_\gamma) + 1}}{C(\gamma)(C_{\mathbf{K},\gamma} + L_\gamma) + 2} \|(\mathbf{u}_{h,\gamma}, \lambda_{h,\gamma})\|_{1,\tau,\star}. \quad (4.34b)$$

This implies that we have

$$\|(\mathbf{v}_{h,\gamma}, \mu_{h,\gamma})\|_{1,\tau,\star} \leq 3 \|(\mathbf{u}_{h,\gamma}, \lambda_{h,\gamma})\|_{1,\tau,\star}. \quad (4.35)$$

This result together with (4.33) leads to (4.23). For the limit case when  $\alpha_\gamma \rightarrow \infty$ , we repeat the same lines as before while using (4.14) instead of (4.7), we promptly arrive to (4.24).  $\square$

**Lemma 4.8 (Well-posedness of the DD scheme).** *The domain decomposition scheme (4.5) is well-posed, and all eigenvalues of the induced system  $\mathcal{A}_\gamma + s_\gamma$  are bounded away from zero.*

*Proof.* The matrix associated to  $\mathcal{A}_\gamma + s_\gamma$  is non-singular, that is to say that the system (4.5) has a unique solution. Moreover, the stability estimate (4.23) (also (4.24)) guarantees that the lowest eigenvalue is bounded away from zero.  $\square$

Let us comment on the robustness of the stability estimate in Theorem 4.7. First, (4.23) states that, regardless of the choice of the space and time discretization, the stability constant with respect to the norm  $\|(\mathbf{u}_{h,\gamma}, \lambda_{h,\gamma})\|_{1,\tau,\star}$  is independent of the coefficients  $\mathbf{K}$ ,  $\mathbf{K}_\gamma$ , and the stabilization parameter  $L_\gamma$ . One can also show that this estimate is asymptotically robust and bounded independently of  $(\tau, \alpha_\gamma, h) \rightarrow 0$  and the stability constant tends to  $1/6$ . The only issue can happen having a large coefficient  $\alpha_\gamma$ , but this case is resolved in (4.24). Therein, as the ratio  $\tau/h \rightarrow 0$ , the stability constant is approximately  $1/6$ .

Following the approach of Ern and Guermond [23], we now provide an estimate for the condition number of the stiffness matrix associated with the domain decomposition system  $\mathcal{A}_\gamma + s_\gamma$ . This condition number estimate is important in our analysis as any algorithm is stable if every step is well-conditioned. This will also encourage the development of the flux basis framework in Section 6. Let us first introduce some basic notation in order to provide the definition of the condition number. We recall the stiffness matrix  $\mathcal{A}_{\text{DD}}$  introduced in (3.2) associated with the domain decomposition scheme (4.5),

$$(\mathcal{A}_{\text{DD}}V, W)_N := \mathcal{A}_\gamma((\mathbf{u}_{h,\gamma}, \lambda_{h,\gamma}), (\mathbf{v}_{h,\gamma}, \mu_{h,\gamma})) + s_\gamma(\lambda_{h,\gamma}, \mu_{h,\gamma}), \quad (4.36)$$

for all  $(\mathbf{u}_{h,\gamma}, \lambda_{h,\gamma}), (\mathbf{v}_{h,\gamma}, \mu_{h,\gamma}) \in \mathbf{V}_{h,\gamma} \times M_{h,\gamma}$ , where  $(V, W)_N := \sum_{i=1}^N V_i W_i$  denotes the inner product in  $\mathbb{R}^N$  and  $|V|_N^2 := (V, V)_N$  is the corresponding Euclidean norm. The condition number is defined by

$$\kappa(\mathcal{A}_{\text{DD}}) := |\mathcal{A}_{\text{DD}}|_N |\mathcal{A}_{\text{DD}}|_N^{-1}, \quad (4.37)$$

where

$$|\mathcal{A}_{\text{DD}}|_N := \sup_{V \in \mathbb{R}^N \setminus \mathbf{0}} \sup_{W \in \mathbb{R}^N \setminus \mathbf{0}} \frac{(\mathcal{A}_{\text{DD}}V, W)_N}{|V|_N |W|_N}, \quad (4.38)$$

which is equivalent to

$$|\mathcal{A}_{\text{DD}}|_N := \sup_{V \in \mathbb{R}^N \setminus \mathbf{0}} \frac{|\mathcal{A}_{\text{DD}}|_N}{|V|_N}. \quad (4.39)$$

We recall the following estimate that holds true for a conforming, quasi-uniform mesh  $\mathcal{T}_h$  [23]; there exists  $c_\mu, C_\mu > 0$  such that the following equivalence holds

$$c_\mu h^{d/2} |V|_N \leq \|V\|_{0,\tau,\star} \leq C_\mu h^{d/2} |V|_N. \quad (4.40)$$

**Theorem 4.9 (Condition number estimate).** *The condition number of the domain decomposition scheme (4.5) is bounded as*

$$\kappa(\mathcal{A}_{\text{DD}}) \lesssim 6(1 + \tau\alpha_\gamma)^2 \max((1 + C_{\text{inv}} c_{\mathbf{K},\gamma} \tau h^{-2}), (1 + \alpha_\gamma \tau)). \quad (4.41)$$

Furthermore, if  $\alpha_\gamma \rightarrow \infty$ ,

$$\kappa(\mathcal{A}_{\text{DD}}) \lesssim 6(1 + C_{\text{dTr}}^2 c_{\mathbf{K}}^{-1} \tau h^{-1})^2 \max((1 + C_{\text{inv}} c_{\mathbf{K},\gamma} \tau h^{-2}), (1 + C_{\text{dTr}}^2 c_{\mathbf{K}}^{-1} \tau h^{-1})). \quad (4.42)$$

*Proof.* We need to bound  $|\mathcal{A}_{\text{DD}}|_N$  and  $|\mathcal{A}_{\text{DD}}|_N^{-1}$ . By definition, for all  $V, W \in \mathbb{R}^N$ ,

$$\begin{aligned} (\mathcal{A}_{\text{DD}}V, W)_N &= \mathcal{A}_\gamma((\mathbf{u}_{h,\gamma}, \lambda_{h,\gamma}), (\mathbf{v}_{h,\gamma}, \mu_{h,\gamma})) + s_\gamma(\lambda_{h,\gamma}, \mu_{h,\gamma}), \\ &\leq \|(\mathbf{u}_{h,\gamma}, \lambda_{h,\gamma})\|_{1,\tau,\star} \|(\mathbf{v}_{h,\gamma}, \mu_{h,\gamma})\|_{1,\tau,\star}, \\ &\leq \max((1 + C_{\text{inv}} c_{\mathbf{K},\gamma} \tau h^{-2}), (1 + \alpha_\gamma \tau)) \|(\mathbf{u}_{h,\gamma}, \lambda_{h,\gamma})\|_{0,\tau,\star} \|(\mathbf{v}_{h,\gamma}, \mu_{h,\gamma})\|_{0,\tau,\star}, \\ &\lesssim \max((1 + C_{\text{inv}} c_{\mathbf{K},\gamma} \tau h^{-2}), (1 + \alpha_\gamma \tau)) h^d |V|_N |W|_N, \end{aligned} \quad (4.43)$$

where the estimate (4.19) and the equivalence (4.40) were successively used. Consequently,

$$|\mathcal{A}_{\text{DD}}|_N \lesssim \max((1 + C_{\text{inv}} c_{\mathbf{K},\gamma} \tau h^{-2}), (1 + \alpha_\gamma \tau)) h^d. \quad (4.44)$$

To estimate  $|\mathcal{A}_{\text{DD}}|_N^{-1}$ , start from (4.23) and use (4.40) to get

$$\begin{aligned} (\mathcal{A}_{\text{DD}}V, W)_N &\geq \frac{1}{6(1 + \tau\alpha_\gamma)^2} \|(\mathbf{u}_{h,\gamma}, \lambda_{h,\gamma})\|_{1,\tau,\star} \|(\mathbf{v}_{h,\gamma}, \mu_{h,\gamma})\|_{1,\tau,\star}, \\ &\geq \frac{1}{6(1 + \tau\alpha_\gamma)^2} \|(\mathbf{u}_{h,\gamma}, \lambda_{h,\gamma})\|_{0,\tau,\star} \|(\mathbf{v}_{h,\gamma}, \mu_{h,\gamma})\|_{0,\tau,\star}, \\ &\gtrsim \frac{h^d}{6(1 + \tau\alpha_\gamma)^2} |V|_N |W|_N, \end{aligned} \quad (4.45)$$

and hence  $|V|_N \lesssim 6(1 + \tau\alpha_\gamma)^2 h^{-d} |\mathcal{A}_{\text{DD}} V|_N$ . Now setting  $V = \mathcal{A}_{\text{DD}}^{-1} W$ , we easily conclude that  $|\mathcal{A}_{\text{DD}}^{-1}|_N \lesssim 6(1 + \tau\alpha_\gamma)^2 h^{-d}$ . Combining estimates for  $|\mathcal{A}_{\text{DD}}^{-1}|_N$  and  $|\mathcal{A}_{\text{DD}}|_N$  we get (4.41). The estimate (4.42) of the limiting case  $\alpha_\gamma \rightarrow \infty$  is obtained similarly by using (4.20) and (4.24) in the proof.  $\square$

## 4.2 Convergence of MoLDD-scheme

The second step of our analysis is to prove the convergence of Algorithm 3.1. The idea is to prove that this algorithm is a contraction and then apply the Banach fixed-point theorem [46]. To this purpose, we let  $\delta_{\mathbf{u},h}^k = \mathbf{u}_{h,\gamma}^{n,k} - \mathbf{u}_{h,\gamma}^{n,k-1}$  and  $\delta_{\lambda,h}^k = \lambda_{h,\gamma}^{n,k} - \lambda_{h,\gamma}^{n,k-1}$  be the differences between the solutions at iteration  $k$  and  $k-1$  of the problem (3.1), respectively.

**Theorem 4.10 (Convergence of MoLDD-scheme).** *Assuming that Assumptions (A1)–(A5) hold true and that  $L_\gamma(\zeta) = L_\xi/2(1 - \zeta)$ , with a parameter  $\zeta \in [0, 1)$ , Algorithm 3.1 defines a contraction given by*

$$\|\delta_{\lambda,h}^k\|_\gamma^2 + \tau\|\delta_{\lambda,h}^k\|_{s,\gamma}^2 + \left(\frac{L_\gamma}{2} + c_{\mathbf{K},\gamma}\right)\tau\|\delta_{\mathbf{u},h}^k\|_\gamma^2 \leq \left(\frac{L_\gamma}{2} - \zeta\xi_m\right)\tau\|\delta_{\mathbf{u},h}^{k-1}\|_\gamma^2, \quad (4.46)$$

where  $\zeta$  is chosen to improve the convergence rate of the scheme. Furthermore, the limit is the unique solution of (2.11).

*Proof.* By subtracting (3.1) at  $k$  from the ones at  $k-1$ , we obtain

$$(\xi(\mathbf{u}_{h,\gamma}^{n,k-1}) - \xi(\mathbf{u}_{h,\gamma}^{n,k-2}), \mathbf{v})_\gamma + L_\gamma(\delta_{\mathbf{u},h}^k - \delta_{\mathbf{u},h}^{k-1}, \mathbf{v})_\gamma + a_\gamma(\delta_{\mathbf{u},h}^k, \mathbf{v}) - b_\gamma(\mathbf{v}, \delta_{\lambda,h}^k) = 0 \quad \forall \mathbf{v} \in \mathbf{V}_{h,\gamma}, \quad (4.47a)$$

$$c_\gamma(\delta_{\lambda,h}^k, \mu) + \tau b_\gamma(\delta_{\mathbf{u},h}^k, \mu) + \tau s_\gamma(\delta_{\lambda,h}^k, \mu) = 0 \quad \forall \mu \in M_{h,\gamma}. \quad (4.47b)$$

Taking  $\mu = \delta_{\lambda,h}^k$  in (4.47b) and  $\mathbf{v} = \tau\delta_{\mathbf{u},h}^k$  in (4.47a) and summing the equations gives

$$\|\delta_{\lambda,h}^k\|_\gamma^2 + \tau\|\delta_{\lambda,h}^k\|_{s,\gamma}^2 + \tau a_\gamma(\delta_{\mathbf{u},h}^k, \mathbf{v}) + \tau(\xi(\mathbf{u}_{h,\gamma}^{n,k-1}) - \xi(\mathbf{u}_{h,\gamma}^{n,k-2}), \delta_{\mathbf{u},h}^k)_\gamma + L_\gamma\tau(\delta_{\mathbf{u},h}^k - \delta_{\mathbf{u},h}^{k-1}, \delta_{\mathbf{u},h}^k)_\gamma = 0.$$

Following [50], we let  $\zeta \in [0, 1)$  and split the third term while applying the lower bound of  $\mathbf{K}_\gamma^{-1}$ ,

$$\begin{aligned} & \|\delta_{\lambda,h}^k\|_\gamma^2 + \tau\|\delta_{\lambda,h}^k\|_{s,\gamma}^2 + c_{\mathbf{K},\gamma}\tau\|\delta_{\mathbf{u},h}^k\|_\gamma^2 + \zeta\tau(\xi(\mathbf{u}_{h,\gamma}^{n,k-1}) - \xi(\mathbf{u}_{h,\gamma}^{n,k-2}), \delta_{\mathbf{u},h}^{k-1})_\gamma \\ & + (1 - \zeta)\tau(\xi(\mathbf{u}_{h,\gamma}^{n,k-1}) - \xi(\mathbf{u}_{h,\gamma}^{n,k-2}), \delta_{\mathbf{u},h}^{k-1})_\gamma + \tau(\xi(\mathbf{u}_{h,\gamma}^{n,k-1}) - \xi(\mathbf{u}_{h,\gamma}^{n,k-2}), \delta_{\mathbf{u},h}^k - \delta_{\mathbf{u},h}^{k-1})_\gamma \\ & + L_\gamma\tau(\delta_{\mathbf{u},h}^k - \delta_{\mathbf{u},h}^{k-1}, \delta_{\mathbf{u},h}^k)_\gamma \leq 0. \end{aligned} \quad (4.48a)$$

We use the monotonicity and Lipschitz continuity of  $\xi$  given by (A1) together with the identity (4.1), to get

$$\begin{aligned} & \|\delta_{\lambda,h}^k\|_\gamma^2 + \tau\|\delta_{\lambda,h}^k\|_{s,\gamma}^2 + c_{\mathbf{K},\gamma}\tau\|\delta_{\mathbf{u},h}^k\|_\gamma^2 + \zeta\xi_m\tau\|\delta_{\mathbf{u},h}^{k-1}\|_\gamma^2 + \frac{(1 - \zeta)}{L_\xi}\tau\|\xi(\mathbf{u}_{h,\gamma}^{n,k-1}) - \xi(\mathbf{u}_{h,\gamma}^{n,k-2})\|_\gamma^2 \\ & + \frac{L_\gamma}{2}\tau\|\delta_{\mathbf{u},h}^k\|_\gamma^2 + \frac{L_\gamma}{2}\tau\|\delta_{\mathbf{u},h}^k - \delta_{\mathbf{u},h}^{k-1}\|_\gamma^2 \leq \frac{L_\gamma}{2}\tau\|\delta_{\mathbf{u},h}^{k-1}\|_\gamma^2 - \tau(\xi(\mathbf{u}_{h,\gamma}^{n,k-1}) - \xi(\mathbf{u}_{h,\gamma}^{n,k-2}), \delta_{\mathbf{u},h}^k - \delta_{\mathbf{u},h}^{k-1})_\gamma. \end{aligned} \quad (4.48b)$$

We apply Young's inequality (4.2) for the last term in the right-hand side to obtain

$$\begin{aligned} & \|\delta_{\lambda,h}^k\|_\gamma^2 + \tau\|\delta_{\lambda,h}^k\|_{s,\gamma}^2 + c_{\mathbf{K},\gamma}\tau\|\delta_{\mathbf{u},h}^k\|_\gamma^2 + \zeta\xi_m\tau\|\delta_{\mathbf{u},h}^{k-1}\|_\gamma^2 \\ & + \frac{(1 - \zeta)}{L_\xi}\tau\|\xi(\mathbf{u}_{h,\gamma}^{n,k-1}) - \xi(\mathbf{u}_{h,\gamma}^{n,k-2})\|_\gamma^2 + \frac{L_\gamma}{2}\tau\|\delta_{\mathbf{u},h}^k\|_\gamma^2 + \frac{L_\gamma}{2}\tau\|\delta_{\mathbf{u},h}^k - \delta_{\mathbf{u},h}^{k-1}\|_\gamma^2 \\ & \leq \frac{L_\gamma}{2}\tau\|\delta_{\mathbf{u},h}^{k-1}\|_\gamma^2 + \frac{L_\gamma}{2}\tau\|\delta_{\mathbf{u},h}^k - \delta_{\mathbf{u},h}^{k-1}\|_\gamma^2 + \frac{1}{2L_\gamma}\tau\|\xi(\mathbf{u}_{h,\gamma}^{n,k-1}) - \xi(\mathbf{u}_{h,\gamma}^{n,k-2})\|_\gamma^2. \end{aligned} \quad (4.48c)$$

We choose  $L_\gamma = L_\xi/2(1 - \zeta)$ , we immediately obtain (4.46). The inequality (4.46) imply that the sequence  $\delta_{\lambda,h}^{n,k}$  tends to 0 in  $L^2(\gamma)$  and  $\delta_{\mathbf{u},h}^k$  tends to 0 in  $\mathbf{L}^2(\gamma)$ . Now we choose  $\mu = \nabla_\tau \cdot \delta_{\mathbf{u},h}^k$  in (4.47b) to obtain

$$\begin{aligned} \tau\|\nabla_\tau \cdot \delta_{\mathbf{u},h}^k\|_\gamma^2 & = -c_\gamma(\delta_{\lambda,h}^k, \nabla_\tau \cdot \delta_{\mathbf{u},h}^k) - \tau s_\gamma(\lambda_{h,\gamma}^{n,k}, \nabla_\tau \cdot \delta_{\mathbf{u},h}^k), \\ & \leq \|\delta_{\lambda,h}^k\|_\gamma \|\nabla_\tau \cdot \delta_{\mathbf{u},h}^k\|_\gamma + \tau\alpha_\gamma \|\delta_{\lambda,h}^k\|_\gamma \|\nabla_\tau \cdot \delta_{\mathbf{u},h}^k\|_\gamma. \end{aligned}$$

Thus,

$$\tau \|\nabla_\tau \cdot \delta_{\mathbf{u},h}^k\|_\gamma \leq (\alpha_\gamma \tau + 1) \|\delta_{\lambda,h}^k\|_\gamma. \quad (4.49)$$

Hence, by (4.46), we have  $\|\nabla_\tau \cdot \delta_{\mathbf{u},h}^k\|_\gamma$  tends to 0 in  $L^2(\gamma)$ . This shows that  $\delta_{\mathbf{u},h}^k$  tends to 0 in  $\mathbf{H}(\text{div}_\tau, \gamma)$ .  $\square$

**Corollary 4.11 (Optimal MoLDD-convergence rate).** *If  $\xi_m > 0$ , the minimum of the convergence rate of Algorithm 3.1 is reached for the optimal parameter*

$$\zeta^* = \arg \min_{0 < \zeta < 1} \rho(\zeta) = 1 + \frac{L_\xi \xi_m - \sqrt{(L_\xi \xi_m)^2 + 4L_\xi \xi_m^2 c_{\mathbf{K},\gamma} + 4L_\xi \xi_m c_{\mathbf{K},\gamma}^2}}{4\xi_m c_{\mathbf{K},\gamma}}, \quad (4.50a)$$

where  $\rho(\zeta)$  is the convergence rate from (4.46),

$$\rho(\zeta) = \frac{L_\gamma - 2\xi_m \zeta}{L_\gamma + 2c_{\mathbf{K},\gamma}} < 1. \quad (4.50b)$$

Therefore, the optimal stabilization parameter is given by

$$L_{\gamma,\text{opt}} = \frac{L_\xi}{2(1 - \zeta^*)}. \quad (4.50c)$$

*Proof.* Plugging  $L_\gamma = L_\xi/2(1 - \zeta)$  in the contraction estimate (4.46) leads to  $\|\delta_{\mathbf{u},h}^k\|_\gamma^2 \leq \rho(\zeta) \|\delta_{\mathbf{u},h}^{k-1}\|_\gamma^2$ , where

$$\rho(\zeta) = \frac{L_\xi - 4(1 - \zeta)\xi_m \zeta}{L_\xi + 4(1 - \zeta)c_{\mathbf{K},\gamma}} < 1, \quad (4.51)$$

which clearly can be minimal when choosing the optimal value of  $\zeta$ . To calculate  $\zeta^*$ , we differentiate (4.51) with respect to  $\zeta$  and infer the resulting roots and we find that the minimum of (4.51) is obtained for the optimal choice given by (4.50a). Replacing back the resulting value into  $L_\gamma(\zeta)$  delivers the optimal stabilization parameter (4.50c).  $\square$

**Lemma 4.12 (Well-posedness of the mixed-dimensional problem).** *There exists a unique solution to the mixed-dimensional problem (2.6).*

*Proof.* Problem (2.11) is equivalent to (2.6). Since we know from Theorem (4.10) that (2.11) has a unique solution, this equivalence implies that (2.6) is uniquely solvable.  $\square$

We continue with some important remarks concerning the results above and the implications to the convergence rate of MoLDD-scheme.

**Remark 4.13 (Dependence of the convergence rate).** *Obviously, the rate of convergence (4.50b) depends only on the strength of the non-linearity (not on the domain decomposition as an inner solver) by means of the Lipschitz constant  $L_\xi$ , the lower bound  $\xi_m$  and the fracture permeability  $\mathbf{K}_\gamma$ . Particularly, the rate is **independent** of the fracture-matrix coupling parameter  $\alpha_\gamma$ , the mesh size  $h$  and the time step  $\tau$ .*

**Remark 4.14 (Global convergence).** *The convergence of MoLDD-scheme is global, i.e. independent of the initialization and particularly of the used inner DD solver (like GMRes). Nevertheless, it is obviously beneficial if one starts MoLDD-scheme iterations with the solution of the last time step.*

## 5 Analysis of ItLDD-scheme

We turn now to the analysis of the iterative LDD-scheme (Algorithm 3.5). In contrast to MoLDD-scheme, in which two levels of calculations (Linearization+DD) are necessary to achieve the required solution, the iterative LDD-scheme treats simultaneously the non-linearity and DD. We introduce  $\delta_{\mathbf{u},h}^k := \mathbf{u}_{h,\gamma}^{n,k} - \mathbf{u}_{h,\gamma}^n$  and  $\delta_{\lambda,h}^k := \lambda_{h,\gamma}^{n,k} - \lambda_{h,\gamma}^n$ , stating the differences between the solution of the problem (3.1) at iteration  $k$  and the solution of the problem (2.11). Thus, the next result is to be understood as the convergence for the combined Linearization-DD processes.



**Theorem 5.1 (Convergence of ItLDD-scheme).** *Assuming that Assumptions (A1)–(A5) hold true and that  $L_{\gamma,u}(\zeta) = L_\xi/2(1-\zeta)$ , where  $\zeta$  is a parameter to be optimized in  $[0,1)$ , and  $L_{\gamma,p} \geq \alpha_\gamma$ , the ItLDD-scheme given by Algorithm 3.5 is linearly convergent. There holds*

$$\begin{aligned} & \left(1 + \tau \frac{L_{\gamma,p}}{2}\right) \|\delta_{\lambda,h}^k\|_\gamma^2 + \frac{\tau}{2} \|\delta_{\lambda,h}^k\|_{s,\gamma}^2 + \left(\frac{L_{\gamma,u}}{2} + c_{\mathbf{K},\gamma}\right) \tau \|\delta_{\mathbf{u},h}^k\|_\gamma^2 \\ & \leq \left(\frac{L_{\gamma,u}}{2} - \zeta \xi_m\right) \tau \|\delta_{\mathbf{u},h}^{k-1}\|_\gamma^2 + \tau \frac{L_{\gamma,p}}{2} \|\delta_{\lambda,h}^{k-1}\|_\gamma^2. \end{aligned} \quad (5.1)$$

*Proof.* By subtracting (3.1) at the iteration  $k$  from (2.11), we obtain

$$(\xi(\mathbf{u}_{h,\gamma}^{n,k-1}) - \xi(\mathbf{u}_{h,\gamma}^n), \mathbf{v})_\gamma + L_{\gamma,u}(\delta_{\lambda,h}^k - \delta_{\mathbf{u},h}^{k-1}, \mathbf{v})_\gamma + a_\gamma(\delta_{\mathbf{u},h}^k, \mathbf{v}) - b_\gamma(\mathbf{v}, \delta_{\lambda,h}^k) = 0 \quad \forall \mathbf{v} \in \mathbf{V}_{h,\gamma}, \quad (5.2a)$$

$$c_\gamma(\delta_{\lambda,h}^k, \mu) + \tau L_{\gamma,p}(\delta_{\lambda,h}^k - \delta_{\lambda,h}^{k-1}, \mu)_\gamma + \tau s_\gamma(\delta_{\lambda,h}^{k-1}, \mu) + \tau b_\gamma(\delta_{\mathbf{u},h}^k, \mu) = 0 \quad \forall \mu \in M_{h,\gamma}. \quad (5.2b)$$

Taking  $\mathbf{v} = \tau \delta_{\mathbf{u},h}^k$  in (5.2a) and  $\mu = \delta_{\lambda,h}^k$  in (5.2b), and summing up the equations gives

$$\begin{aligned} & \|\delta_{\lambda,h}^k\|_\gamma^2 + \tau L_{\gamma,p}(\delta_{\lambda,h}^k - \delta_{\lambda,h}^{k-1}, \delta_{\lambda,h}^k)_\gamma + \tau s_\gamma(\delta_{\lambda,h}^{k-1}, \delta_{\lambda,h}^k) \\ & + \tau(\xi(\mathbf{u}_{h,\gamma}^{n,k-1}) - \xi(\mathbf{u}_{h,\gamma}^n), \delta_{\mathbf{u},h}^k)_\gamma + L_{\gamma,u}\tau(\delta_{\mathbf{u},h}^k - \delta_{\mathbf{u},h}^{k-1}, \delta_{\mathbf{u},h}^k)_\gamma + \tau a_\gamma(\delta_{\mathbf{u},h}^k, \delta_{\mathbf{u},h}^k) = 0. \end{aligned} \quad (5.3)$$

For any  $\zeta \in [0,1)$ , this is equivalent to,

$$\begin{aligned} & \|\delta_{\lambda,h}^k\|_\gamma^2 + \tau L_{\gamma,p}(\delta_{\lambda,h}^k - \delta_{\lambda,h}^{k-1}, \delta_{\lambda,h}^k)_\gamma + \tau s_\gamma(\delta_{\lambda,h}^k, \delta_{\lambda,h}^k) + \tau \zeta(\xi(\mathbf{u}_{h,\gamma}^{n,k-1}) - \xi(\mathbf{u}_{h,\gamma}^n), \delta_{\mathbf{u},h}^{k-1})_\gamma \\ & + \tau(1-\zeta)(\xi(\mathbf{u}_{h,\gamma}^{n,k-1}) - \xi(\mathbf{u}_{h,\gamma}^n), \delta_{\mathbf{u},h}^{k-1})_\gamma + L_{\gamma,u}\tau(\delta_{\mathbf{u},h}^k - \delta_{\mathbf{u},h}^{k-1}, \delta_{\mathbf{u},h}^k)_\gamma + \tau a_\gamma(\delta_{\mathbf{u},h}^k, \delta_{\mathbf{u},h}^k) \\ & = -\tau s_\gamma(\delta_{\lambda,h}^{k-1} - \delta_{\lambda,h}^k, \delta_{\lambda,h}^k)_\gamma - \tau(\xi(\mathbf{u}_{h,\gamma}^{n,k-1}) - \xi(\mathbf{u}_{h,\gamma}^n), \delta_{\mathbf{u},h}^k - \delta_{\mathbf{u},h}^{k-1})_\gamma. \end{aligned} \quad (5.4)$$

We apply the lower bound in the last term of the left-hand side and then use the monotonicity and Lipschitz continuity of the operator  $\xi$ , followed by Cauchy-Schwarz and Young's inequalities in the second term of the right-hand side, to get

$$\begin{aligned} & \left(1 + \tau \frac{L_{\gamma,p}}{2}\right) \|\delta_{\lambda,h}^k\|_\gamma^2 + \tau \|\delta_{\lambda,h}^k\|_{s,\gamma}^2 + \tau \frac{L_{\gamma,p}}{2} \|\delta_{\lambda,h}^k - \delta_{\lambda,h}^{k-1}\|_\gamma^2 + c_{\mathbf{K},\gamma} \tau \|\delta_{\mathbf{u},h}^k\|_\gamma^2 + \zeta \xi_m \|\delta_{\mathbf{u},h}^{k-1}\|_\gamma^2 \\ & + \frac{(1-\zeta)}{L_\xi} \tau \|\xi(\mathbf{u}_{h,\gamma}^{n,k-1}) - \xi(\mathbf{u}_{h,\gamma}^n)\|_\gamma^2 + \frac{L_{\gamma,u}}{2} \tau \|\delta_{\mathbf{u},h}^k\|_\gamma^2 + \frac{L_{\gamma,u}}{2} \tau \|\delta_{\mathbf{u},h}^k - \delta_{\mathbf{u},h}^{k-1}\|_\gamma^2 \\ & \leq \frac{L_{\gamma,u}}{2} \tau \|\delta_{\mathbf{u},h}^{k-1}\|_\gamma^2 + \frac{L_{\gamma,p}}{2} \tau \|\delta_{\lambda,h}^{k-1}\|_\gamma^2 + \frac{L_{\gamma,u}}{2} \tau \|\delta_{\mathbf{u},h}^k - \delta_{\mathbf{u},h}^{k-1}\|_\gamma^2 - \tau s_\gamma(\delta_{\lambda,h}^{k-1} - \delta_{\lambda,h}^k, \delta_{\lambda,h}^k) \\ & + \frac{1}{2L_{\gamma,u}} \tau \|\xi(\mathbf{u}_{h,\gamma}^{k-1}) - \xi(\mathbf{u}_{h,\gamma}^n)\|_\gamma^2. \end{aligned} \quad (5.5)$$

The continuity of  $s_\gamma$  gives

$$|s_\gamma(\delta_{\lambda,h}^{k-1} - \delta_{\lambda,h}^k, \delta_{\lambda,h}^k)| \leq \|\delta_{\lambda,h}^k\|_{s,\gamma} \|\delta_{\lambda,h}^k - \delta_{\lambda,h}^{k-1}\|_{s,\gamma} \leq \alpha_\gamma^{1/2} \|\delta_{\lambda,h}^k\|_{s,\gamma} \|\delta_{\lambda,h}^k - \delta_{\lambda,h}^{k-1}\|_\gamma, \quad (5.6)$$

where we have used (4.7). Applying Young's inequality to (5.6) and plugging the result in (5.5), then choose  $L_{\gamma,u} = L_\xi/2(1-\zeta)$ , it is inferred,

$$\begin{aligned} & \left(1 + \tau \frac{L_{\gamma,p}}{2}\right) \|\delta_{\lambda,h}^k\|_\gamma^2 + \tau \|\delta_{\lambda,h}^k\|_{s,\gamma}^2 + \tau \frac{L_{\gamma,p}}{2} \|\delta_{\lambda,h}^k - \delta_{\lambda,h}^{k-1}\|_\gamma^2 + \left(\frac{L_{\gamma,u}}{2} + c_{\mathbf{K},\gamma}\right) \tau \|\delta_{\mathbf{u},h}^k\|_\gamma^2 \\ & \leq \left(\frac{L_{\gamma,u}}{2} - \zeta \xi_m\right) \tau \|\delta_{\mathbf{u},h}^{k-1}\|_\gamma^2 + \tau \frac{L_{\gamma,p}}{2} \|\delta_{\lambda,h}^{k-1}\|_\gamma^2 + \tau \frac{\alpha_\gamma}{2} \|\delta_{\lambda,h}^{k-1} - \delta_{\lambda,h}^k\|_\gamma^2 + \frac{\tau}{2} \|\delta_{\lambda,h}^k\|_{s,\gamma}^2. \end{aligned} \quad (5.7)$$

We let  $L_{\gamma,p} \geq \alpha_\gamma$ , to obtain the estimate (5.1) which is clearly a contraction. We finally repeat the same techniques as in (4.49), to get that  $\|\nabla_\tau \cdot \delta_{\mathbf{u},h}^k\|_\gamma$  tends to 0 in  $L^2(\gamma)$ . This altogether shows that  $\delta_{\lambda,h}^{n,k}$  tends to 0 in  $L^2(\gamma)$  and  $\delta_{\mathbf{u},h}^k$  tends to 0 in  $\mathbf{H}(\text{div}_\tau, \gamma)$ .  $\square$

**Remark 5.2 (Contraction factor).** Our contraction estimate shows that the strength of the non-linearity and the matrix fracture (DD) coupling controls the convergence rate. In practice, the contraction factor is better if we take into account the energy norm  $\tau \|\delta_{\lambda,h}^k\|_{s,\gamma}^2/2$  using the bound (4.7). As the stabilization term is such that  $L_{\gamma,p} \geq \alpha_\gamma$ , thus, we have to study the robustness of the algorithm when  $\alpha_\gamma \rightarrow \infty$ , corresponding physically to the case of continuous pressure across the fracture.

**Lemma 5.3 (Contraction-robustness).** Assuming continuous pressure across  $\gamma$  ( $\alpha_\gamma \rightarrow \infty$ ), then let  $L_{\gamma,u}(\zeta) = L_\xi/2(1 - \zeta)$  with  $\zeta$  to be chosen in  $[0, 1)$ , and  $L_{\gamma,p} \geq C_{\text{dTr}}^2/(c_{\mathbf{K}}h)$ , the contraction (5.1) holds true for the ItLDD-scheme in Algorithm 3.5.

*Proof.* Recall the estimate (5.5) which holds true in that case. We then estimate the coupling term  $|s_\gamma(\delta_{\lambda,h}^k - \delta_{\lambda,h}^{k-1}, \delta_{\lambda,h}^k)|$  with the help of (4.14),

$$|s_\gamma(\delta_{\lambda,h}^k - \delta_{\lambda,h}^{k-1}, \delta_{\lambda,h}^k)| \leq \|\delta_{\lambda,h}^k\|_{s,\gamma} \|\delta_{\lambda,h}^k - \delta_{\lambda,h}^{k-1}\|_{s,\gamma} \leq C_{\text{dTr}} c_{\mathbf{K}}^{-1/2} h^{-1/2} \|\delta_{\lambda,h}^k\|_{s,\gamma} \|\delta_{\lambda,h}^k - \delta_{\lambda,h}^{k-1}\|_\gamma. \quad (5.8)$$

We apply Young's inequality to (5.6) and replace the result in (5.5), while choosing  $L_\gamma = L_\xi/2(1 - \zeta)$ ,

$$\begin{aligned} & \left(1 + \tau \frac{L_{\gamma,p}}{2}\right) \|\delta_{\lambda,h}^k\|_\gamma^2 + \tau \|\delta_{\lambda,h}^k\|_{s,\gamma}^2 + \tau \frac{L_{\gamma,p}}{2} \|\delta_{\lambda,h}^k - \delta_{\lambda,h}^{k-1}\|_\gamma^2 + \left(\frac{L_{\gamma,u}}{2} + c_{\mathbf{K},\gamma}\right) \tau \|\delta_{\mathbf{u},h}^k\|_\gamma^2 \\ & \leq \left(\frac{L_{\gamma,u}}{2} - \zeta \xi_m\right) \tau \|\delta_{\mathbf{u},h}^{k-1}\|_\gamma^2 + \frac{L_{\gamma,p}}{2} \tau \|\delta_{\lambda,h}^{k-1}\|_\gamma^2 + \frac{C_{\text{dTr}}^2}{c_{\mathbf{K}}} h^{-1} \frac{\tau}{2} \|\delta_{\lambda,h}^{k-1} - \delta_{\lambda,h}^k\|_\gamma^2 + \frac{\tau}{2} \|\delta_{\lambda,h}^k\|_{s,\gamma}^2. \end{aligned}$$

We choose  $L_{\gamma,p} \geq C_{\text{dTr}}^2/(c_{\mathbf{K}}h)$ , we end up with the contraction (5.1). The rest of the proof is as in Theorem 5.1.  $\square$

We complete our analysis of Algorithm 3.5 by giving alternative convergence results when  $(h, 1/\alpha_\gamma) \rightarrow 0$ , leading to extremely large stabilization parameter  $L_{\gamma,p}$ , which deteriorates the convergence rate of ItLDD scheme. These results are then important to show the robustness of the iterative LDD-scheme for extreme physical and/or discretization situations.

**Proposition 5.4 (Alternative convergence results).** If  $L_{\gamma,p} = 0$ , and  $L_{\gamma,u} = L_\xi/2(1 - \zeta)$  with  $\zeta \in [0, 1)$ , Algorithm 3.5 is convergent under the constraint on the time step  $\tau \leq 1/\alpha_\gamma$ . The following estimate for Algorithm 3.5 holds true and defines a contraction

$$\left(1 - \frac{\alpha_\gamma}{2} \tau\right) \|\delta_{\lambda,h}^k\|_\gamma^2 + \left(\frac{L_{\gamma,u}}{2} + c_{\mathbf{K},\gamma}\right) \tau \|\delta_{\mathbf{u},h}^k\|_\gamma^2 \leq \left(\frac{L_{\gamma,u}}{2} - \zeta \xi_m\right) \tau \|\delta_{\mathbf{u},h}^{k-1}\|_\gamma^2 + \frac{\alpha_\gamma}{2} \tau \|\delta_{\lambda,h}^{k-1}\|_\gamma^2. \quad (5.9)$$

Moreover, if  $\alpha_\gamma \rightarrow \infty$ , Algorithm 3.5 is convergent as the ratio  $\tau/h \leq c_{\mathbf{K}}/C_{\text{dTr}}^2 (= C_{\gamma,s}^{-1})$  holds true, and the resulting estimate is a contraction given by

$$\left(1 - \frac{C_{\gamma,s}}{2} \frac{\tau}{h}\right) \|\delta_{\lambda,h}^k\|_\gamma^2 + \left(\frac{L_{\gamma,u}}{2} + c_{\mathbf{K},\gamma}\right) \tau \|\delta_{\mathbf{u},h}^k\|_\gamma^2 \leq \left(\frac{L_{\gamma,u}}{2} - \zeta \xi_m\right) \tau \|\delta_{\mathbf{u},h}^{k-1}\|_\gamma^2 + \frac{C_{\gamma,s}}{2} \frac{\tau}{h} \|\delta_{\lambda,h}^{k-1}\|_\gamma^2. \quad (5.10)$$

*Proof.* We let  $L_{\gamma,p} = 0$  in the estimate (5.3) to get

$$\|\delta_{\lambda,h}^k\|_\gamma^2 + \tau(b_\gamma(\mathbf{u}_{h,\gamma}^{n,k-1}) - b_\gamma(\mathbf{u}_{h,\gamma}^n), \delta_{\mathbf{u},h}^k)_\gamma + L_{\gamma,u} \tau (\delta_{\mathbf{u},h}^k - \delta_{\mathbf{u},h}^{k-1}, \delta_{\mathbf{u},h}^k)_\gamma + \tau a_\gamma(\delta_{\mathbf{u},h}^k, \delta_{\mathbf{u},h}^k) = -\tau s_\gamma(\delta_{\lambda,h}^{k-1}, \delta_{\lambda,h}^k).$$

With the same techniques used to get (5.5), we get for  $L_{\gamma,u} = L_\xi/2(1 - \zeta)$  with  $\zeta \in [0, 1)$ ,

$$\begin{aligned} & \left(1 + \tau \frac{L_{\gamma,p}}{2}\right) \|\delta_{\lambda,h}^k\|_\gamma^2 + \tau \|\delta_{\lambda,h}^k\|_{s,\gamma}^2 + \left(\frac{L_{\gamma,u}}{2} + c_{\mathbf{K},\gamma}\right) \tau \|\delta_{\mathbf{u},h}^k\|_\gamma^2 \\ & \leq \left(\frac{L_{\gamma,u}}{2} - \zeta \xi_m\right) \tau \|\delta_{\mathbf{u},h}^{k-1}\|_\gamma^2 - \tau s_\gamma(\delta_{\lambda,h}^{k-1}, \delta_{\lambda,h}^k). \end{aligned} \quad (5.11)$$

The coupling term in the right-hand side is now estimated as follows

$$|s_\gamma(\delta_{\lambda,h}^{k-1}, \delta_{\lambda,h}^k)| \leq \alpha_\gamma \|\delta_{\lambda,h}^{k-1}\|_\gamma \|\delta_{\lambda,h}^k\|_\gamma,$$

where we used (4.7). Applying Young inequality and inserting the result in (5.11), we infer (5.9). That of the second estimate (5.10), when  $\alpha_\gamma \rightarrow \infty$ , is obtained similarly to (5.9), but with using (4.14) to bound the coupling term.  $\square$

**Remark 5.5 (Time step vs stabilization).** *The constraint on the ratio  $\tau/h$  is less restrictive than the constrain on the stabilization parameter  $L_{\gamma,p}$  in Lemma 5.3. We also note that the constraint on the time step  $\tau \leq 1/\alpha_\gamma$  may have the same implication on the convergence rate as taking  $L_{\gamma,p} \geq \alpha_\gamma$  in Theorem 5.1. In practice, the choice between the two constraints may depend on the physical situation. All the results show a strong correlation between the Robin parameter  $\alpha_\gamma$ , and the time step  $\tau$  (or  $\tau/h$ ) or the stabilization parameter  $L_{\gamma,p}$ .*

## 6 The LDD Iterations with Multiscale Flux Basis Implementation

In this section, we propose an alternative to the matrix-free method (see Subsection 3.1) by forming the inter-dimensional map  $\mathcal{S}_\gamma^{\text{RtN}}$  based on the construction of a multiscale mortar flux basis (MFB) from [1, 31]. We recall that the goal of this paper is to solve the reduced scheme of Definition 2.2 for: 1) different physical parameters and various realizations of the  $L$ -scheme parameters, 2) various PDEs by changing the non-linearity  $\xi$ , and 3) when computing and comparing the two LDD solvers (MoLDD *vs* ItLDD). We also recall that the dominant computational cost in the LDD algorithms comes from the subdomain solves to evaluate the action of  $\mathcal{S}_\gamma^{\text{RtN}}$  using Algorithm 3.3 (step 2(b)). These solves are required at each inner and outer iterations of Algorithm 3.1 and each iteration of Algorithm 3.5 (see Remark 3.4 and 3.6 for the overall cost). Therefore, the computation cost of the algorithms may become large since, first, the LDD solver may require a large number of iterations for complex problems, and second, we have seen that the condition number (4.41)-(4.42) of the linearized interface problem grows with refining the grids or increasing  $\alpha_\gamma$  (normal permeability) and permeability contrast.

The construction of the inter-dimensional mapping is achieved by pre-computing and storing the flux subdomain responses, called *multiscale flux basis*, associated with each fracture pressure degree of freedom on each subdomain. We define  $(\Phi_{h,\gamma}^\ell)_{\ell=1}^{\mathcal{N}_{h,\gamma}}$  to be the set of basis functions on the interface pressure space  $M_{h,\gamma}$ , where  $\mathcal{N}_{h,\gamma}$  is the number of pressure degrees of freedom on  $\gamma$  [32]. As a result, on the fracture interface, we let  $\mu_{h,\gamma} := \sum_{\ell=1}^{\mathcal{N}_{h,\gamma}} \mu_{h,\gamma}^\ell \Phi_{h,\gamma}^\ell$ , and compute the MFB functions corresponding to  $(\Phi_{h,\gamma}^\ell)_{\ell=1}^{\mathcal{N}_{h,\gamma}}$  using the following algorithm:

**Algorithm 6.1 (Assembly of the multiscale flux basis).**

1. Enter the basis  $(\Phi_{h,\gamma}^\ell)_{\ell=1}^{\mathcal{N}_{h,\gamma}}$ . Set  $\ell := 0$ .
2. **Do**
  - (a) Increase  $\ell := \ell + 1$ .
  - (b) Project  $\Phi_{h,\gamma}^\ell$  on the subdomain boundary,  $\lambda_{h,i}^\ell = \mathcal{Q}_{h,i}(\Phi_{h,\gamma}^\ell)$ .
  - (c) Solve problem (2.8) in each subdomain  $\Omega_i$ .
  - (d) Project the resulting flux onto the pressure space on the fracture,  $\Psi_{h,\gamma,i}^\ell := -\mathcal{Q}_{h,i}^T \mathbf{u}_{h,i}^* (\lambda_{h,i}^\ell) \cdot \mathbf{n}_i$ .

**While**  $\ell \leq \mathcal{N}_{h,\gamma}$ .

3. Form the multiscale flux basis for subdomain  $\Omega_i$ , i.e.,  $\{\Psi_{h,\gamma,i}^1, \Psi_{h,\gamma,i}^2, \dots, \Psi_{h,\gamma,i}^{\mathcal{N}_{h,\gamma}}\} \subset M_{h,\gamma}$ .

Once the multiscale flux basis functions are constructed for each subdomain, the action of  $\mathcal{S}_\gamma^{\text{RtN}}$  is replaced by a linear combination of the multiscale flux basis functions  $\Psi_{h,\gamma,i}^\ell$ . Specifically, at any time step  $n \geq 1$ , and at any iteration  $m \geq 1$  of any of the algorithms, for an interface datum  $\lambda_{h,\gamma}^{n,m} \in M_{h,\gamma}$ , we have  $\lambda_{h,\gamma}^{n,m} = \sum_{\ell=1}^{\mathcal{N}_{h,\gamma}} \lambda_{h,\gamma}^{n,m,\ell} \Phi_{h,\gamma}^\ell$ , and for  $i \in \{1, 2\}$ ,

$$\mathcal{S}_{\gamma,i}^{\text{RtN}}(\lambda_{h,\gamma}^{n,m}) = \sum_{\ell=1}^{\mathcal{N}_{h,\gamma}} \lambda_{h,\gamma}^{n,m,\ell} \mathcal{S}_{\gamma,i}^{\text{RtN}}(\Phi_{h,\gamma}^\ell) = \sum_{\ell=1}^{\mathcal{N}_{h,\gamma}} \lambda_{h,\gamma}^{n,m,\ell} \Psi_{h,\gamma,i}^\ell. \quad (6.1a)$$

We then compute the jump across the fracture

$$\mathcal{S}_\gamma^{\text{RtN}}(\lambda_{h,\gamma}^{n,m}) = \sum_{i \in \{1,2\}} \mathcal{S}_{\gamma,i}^{\text{RtN}}(\lambda_{h,\gamma}^{n,m}). \quad (6.1b)$$

We continue with some important remarks on the applicability of the MFB.

**Remark 6.2 (Fracture network).** We observe that each fracture pressure basis function  $\Phi_{h,\gamma}^\ell$  on the fracture interface corresponds to exactly two different multiscale flux basis functions, one for  $\Omega_1$  and one for  $\Omega_2$ . For the case of a fracture network, say  $\gamma = \cup_{i \neq j} \gamma_{ij}$ , where  $\gamma_{ij}$  is the fracture between the subdomain  $\Omega_i$  and  $\Omega_j$ , the previous basis reconstruction is then applied independently on each fracture.

**Remark 6.3 (On the MFB - gain).** Note that (6.1) permits now retrieving the action of  $\mathcal{S}_\gamma^{\text{RtN}}$  on  $M_{h,\gamma}$ , for **any outer or inner iteration of the LDD solvers**, and **for all time steps**  $n \in \{1, 2, \dots, N\}$ . Thus, the use of MFB eliminates the dependence between the total number of subdomain solves and the number of iterations of each LDD solver.

**Remark 6.4 (On the MFB - cost).** For large scale simulations, the multiscale (Robin-to-Neumann) functions are stored on the subdomain level then on different processors, so that the inter-dimensional mapping  $\mathcal{S}_\gamma^{\text{RtN}}$  need not be assembled. As detailed in Subsection 3.1, a Krylov method is used to solve for the GMRes update in (3.3) (for (3.4) for the ItLDD solver) which requires only the action of the Robin-to-Neumann operator on each Krylov vector. We have explained through the paper that, with constructing the operator  $\mathcal{S}_\gamma^{\text{RtN}}$ , the cost in solving the problem is much smaller than the cost of solving subdomain problems [1], where the only issue being the storage capacity. Precisely, the cost of the MFB is associated with constructing the  $\mathcal{S}_\gamma^{\text{RtN}}$  directly depends on the number of degrees of freedom on the fractures. Thus, the MFB framework is favourable for 1) highly heterogeneous parts of the media where subdomain solves are affected by heterogeneities, 2) those fractures affected by strong non-linearities, and 3) lower permeable or blocking fractures where a coarse mortar space can be used without sacrificing accuracy. Otherwise, a robust preconditioner [7, 18] can be used in the Krylov method, as well as a coarse mortar space that is compensated by taking higher order mortars [9, 55].

## 7 Numerical examples

In this section, we present several test cases to show how the schemes behave (1) for different values for numerical and physical parameters (2) with coarsening/refining mortar grids (3) on extensions to other governing equations. We subsequently study the value of  $L_{\gamma, \text{opt}}$  in the MoLDD scheme and the relationship between  $L_{\gamma, u}$  and  $L_{\gamma, p}$  in the ItLDD scheme. The performance of schemes is measured in the overall number of iterations needed for each scheme to reach the stopping criteria. In the implementation of both schemes, we consider that the solution has converged if the relative error of the fracture solution is less than  $10^{-5}$ , if the value at the previous iteration step is not zero. Otherwise we use the absolute error.

To keep the presentation simple, we consider domain and several parameters in common in all the examples in relation to the first test case in [43]. The domain  $\Omega := (0, 2) \times (0, 1)$  is intersected with a fracture defined as  $\gamma := \{x = 1\}$ . On the boundaries of the rock matrix  $\{x = 0\}$  and  $\{x = 2\}$  we impose pressure boundary condition with values 0 and 1, respectively. We set zero flux boundary condition on the rest of  $\partial\Omega$ . The boundary of the fracture at the tips  $\{y = 1\} \cap \partial\gamma$  and  $\{y = 0\} \cap \partial\gamma$  inherits the pressure boundary conditions from the rock matrix. The examples are set on the time interval  $I = (0, 1)$  with homogeneous pressure initial condition. As for the physical parameters, we take the permeability matrix for the bulk  $\mathbf{K}_i = \mathbf{I}$ , while the source terms  $f_i$  and  $f_\gamma$  are equal to zero.

**Remark 7.1 (On the inner DD solver).** Previously we have mentioned the computational cost of both methods in the context of an iterative Krylov solver. However, the following examples are reduced to a one-dimensional fracture problem with negligible number of degrees of freedom (DOF) for such a solver to perform efficiently. Therefore, we only use the direct methods to solve the interface problem and rather demonstrate the robustness of our methods with regards to discretization, temporal, physical and L-scheme parameters. We still emphasize the need for a Krylov solver, such as GMRes, for large-scale problems.

First, we consider the Forchheimer flow model where the non linear term is  $\xi(\mathbf{u}_\gamma) = \beta|\mathbf{u}_\gamma|\mathbf{u}_\gamma$ . The parameter  $\beta$  is a fluid dependent non-negative scalar known as the Forchheimer coefficient, and  $|\cdot|$  denotes the Euclidean vector norm  $|\mathbf{u}_\gamma|^2 = \mathbf{u}_\gamma \cdot \mathbf{u}_\gamma$ . It is straightforward to see that  $\xi$  is a simply increasing function and satisfies condition (A1). For more details see [33, 38] and references therein.

$h \backslash n$	1	2	3	4	5	$\tau$																
$2^{-1}$	17	12	11	10	9	$2^{-2}$	17				11				10				9			
$2^{-3}$	17	11	10	9	8	$2^{-3}$	17		10		9		9		8		8		7		6	
$2^{-5}$	17	11	10	9	8	$2^{-4}$	16	10	9	9	9	8	8	8	7	7	7	6	6	6	5	5

$h \backslash n$	1	2	3	4	5	$\tau$																
$2^{-1}$	17	8	7	7	6	$2^{-2}$	17				9				8				7			
$2^{-3}$	17	9	8	7	7	$2^{-3}$	17		10		9		8		8		7		6		6	
$2^{-5}$	17	9	8	7	7	$2^{-4}$	16	10	9	9	9	8	8	8	7	7	7	6	6	6	5	5

Table 1: Results for the example of Subsection 7.1. Top two tables correspond to solving with the MoLDD scheme, while bottom two correspond to solving with the ItLDD scheme. On the left we report the number of iterations by varying the mesh size  $h$  for a fixed time step  $\tau = 2^{-4}$ , while on the right depending on the time step size  $\tau$  for a fixed mesh size  $h = 2^{-5}$ .

## 7.1 Stability with respect to the user-given parameters

We first study the performances of MoLDD and ItLDD solvers by varying the time step  $\tau$ , the mesh size  $h$ , and the  $L$ -scheme parameters  $(L_{\gamma,u}, L_{\gamma,p})$ . We let  $\mathbf{K}_\gamma = 1$ ,  $\alpha_\gamma = 10^4$  and  $\beta = 1$  and according to the theoretical results, the  $L$ -scheme parameters are given by  $L_{\gamma,u} \approx 1$  and  $L_{\gamma,p} = 10^3$ . Results in Table 1 report the number of iterations required by the two LDD solvers while varying the mesh size  $h$  and time step size  $\tau$ . Each column of the tables represent results for a time step  $n$ .

Regardless of the choice of scheme, we can observe that the number of iterations is independent from the mesh size and slightly dependent on the time step size. The reason for the latter might be related to the fact that we consider the solution at previous iteration as the initial guess for the next iteration. Thus, by decreasing the time step size, the variation of the solution between steps varies less and so the number of iterations. Overall, the sequential ItLDD and the monolithic MoLDD solvers behave similarly; one can also see a slightly better results for the iterative solver in Table 1 (left). Note that any comparison of the two solvers does not make sense for the simple reason that the amounts of stabilization fixed by  $L_{\gamma,p}$  and  $L_{\gamma,u}$  are not yet optimal. Another explanation, may also be, the amount of stabilization in the monolithic solver MoLDD is set solely by  $L_{\gamma,u}$ , in contrast to the iterative solver ItLDD where two stabilization parameters  $L_{\gamma,p}$  and  $L_{\gamma,u}$  are used.

Finally, we recall that with the use of the multiscale flux basis, the computational costs of the two solvers is practically the same. In other words, any computational overhead of any of the solvers is free from any additional costs. The main cost is done offline using the multiscale flux basis which is mostly related to the number of mortar degrees on the fracture. As an example, the computational cost needed to draw the results in the last line (for  $h = 2^{-5}$ ) of the two right tables (in Table 1) is approximately equal to 96 subdomain solves (Num. of DOF \* Num. of subdo. +  $2 * N$ ), where two solves per time step are required to form the right-hand side in (3.1) (for MoLDD) and (3.4) (for ItLDD). Without MBF, the cost should be  $\sum_{n=1}^N \sum_{k=1}^{N_{\text{Lin}}^n} * N_{\text{dd}}^k + 2 * N$ , where  $N_{\text{Lin}}^n$  is the number of iterations of the  $L$ -scheme, and  $N_{\text{dd}}^k$  denotes the number of DD iterations (GMRes or any Krylov solver). Thus, if we assume a fixed  $N_{\text{dd}}^k$  along all the simulation, say  $N_{\text{dd}}^k = 2$ , this number will be at least 1012 subdomain solves, so that with MFB, we make a save of approximately 91% of the total subdomain solves.

In Figure 1, we plot the number of iterations with various realizations of the user-given  $L_{\gamma,u}$  in MoLDD solver. We consider 100 values of  $L_{\gamma,u}$ , from 0 to 2.5 with uniform step 0.025. The other parameters are fixed as follows,  $\beta = 1$ ,  $h = 0.125$  and  $\tau = 0.2$ . The graph in this figure behaves very similarly to what is usually observed for the  $L$ -type schemes (a typical V-shape graph), highlighting a numerically optimal value  $L_{\gamma,\text{opt}}$  between 0.5 and 1. By increasing  $L_{\gamma,u}$ , the number of iterations slowly increases, while they increase more drastically for small value of  $L_{\gamma,u}$ . This behavior is common for all time steps. We expect such a behavior when choosing  $L_{\gamma,u}$  close to zero because it directly influences the contraction factor in (4.46). As a side result, we can see that the identified parameter  $L_{\gamma,\text{opt}} \approx 1$  is close to the optimal one. On the other hand, we can observe the performance of the ItLDD solver with regards to changing parameters  $L_{\gamma,u}$  and  $L_{\gamma,p}$ . We consider  $L_{\gamma,u}$  taking 50 values uniformly distributed on the interval  $(0, 2.5)$ , while  $L_{\gamma,p} = 10^x$ , where  $x$  are 21 equidistant values on the interval  $(2.2, 4.2)$  with step 0.1. As in the previous figure, we can observe

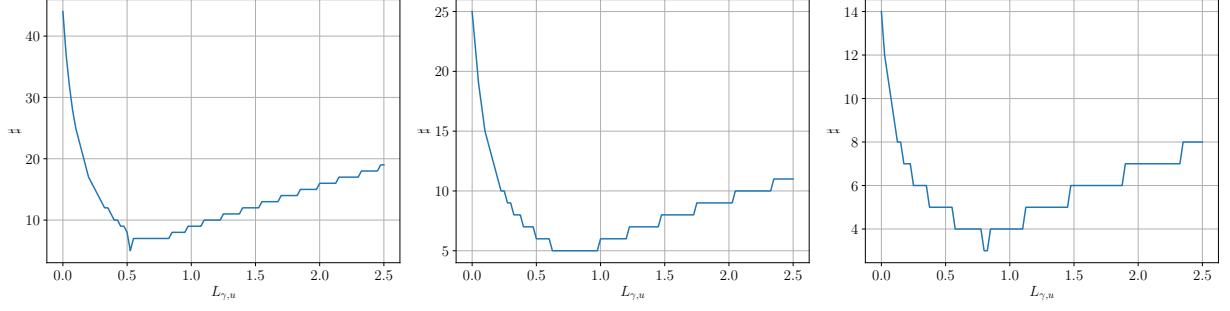


Figure 1: Results for the example of Subsection 7.1 using MoLDD scheme. We report the number of iterations  $\sharp$  for different values of  $L_{\gamma,u}$ . On the left for the first time step, in the centre for the third, and on the right for the last time step.

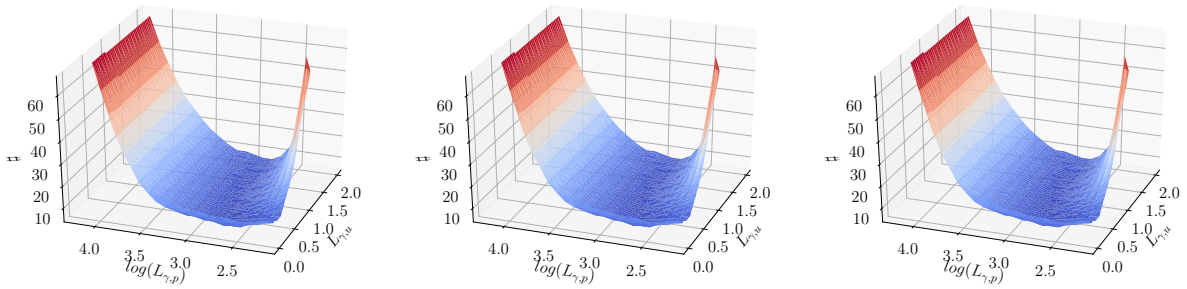


Figure 2: Results for the example of Subsection 7.1 using ItLDD scheme. We report the number of iterations  $\sharp$  for different values of  $L_{\gamma,u}$  and  $L_{\gamma,p}$ . On the left for the first time step, in the centre for the third, and on the right for the last time step.

$\beta \backslash n$	1	2	3	4	5
0.1	17	9	8	7	7
1	17	9	8	7	7
100	9	8	7	6	5

$\beta \backslash n$	1	2	3	4	5
0.1	17	11	10	9	8
1	17	11	10	9	8
100	14	10	9	9	8

$\alpha_\gamma \backslash n$	1	2	3	4	5
$10^2$	17	9	8	7	7
$10^4$	17	9	8	7	7
$10^6$	17	9	8	7	7
$10^8$	17	9	8	7	7

$\alpha_\gamma \backslash n$	1	2	3	4	5
$10^2$	17	11	10	9	9
$10^4$	17	11	10	9	8
$10^6$	17	11	10	9	8
$10^8$	17	11	10	9	8

Table 2: Results for the example of Subsection 7.2 reporting the number of iterations by varying the parameter  $\beta$  (top) and by varying  $\alpha_\gamma$  (bottom). Left tables correspond to solving with the MoLDD solver, while the right ones correspond to solving with the ItLDD solver.

on the surface plots that there is a global minimum that determines the optimal choice for  $L_{\gamma,u}$  and  $L_{\gamma,p}$ . For example, the minimum number of iterations for this flow model is 5 for  $L_{\gamma,u}$  between 0.59 and 1.1 and  $\log(L_{\gamma,p})$  between 2.8 and 3, in all time steps. Similar to the monolithic approach, the number of iterations required by the ItLDD solver increases when the L-scheme parameters assume low values. Particularly, the scheme diverges when  $L_{\gamma,p}$  is less or equal to  $10^2$ . In the analysis of the scheme we require that  $L_{\gamma,p} \geq \alpha_\gamma$ , but the lower values also allow a good convergence behaviour concluding that the theoretical lower bound is possibly too strict, but it certainly exists. Therefore, in practice, we can slightly relax the bounds on the L-scheme parameters to still obtain good performance of the solver. It is also relevant to mention that the normal permeability constant  $\alpha_\gamma = 10^4$  is sufficiently large to apply the limit case results in Lemma 5.3.

Crucially, we want to mention that the computational cost of the realizations needed to draw Figure 1 and 2, is exactly equal to only one realization with fixed  $(L_{\gamma,u}, L_{\gamma,p})$ , permitting easier calculation of these parameters, and confirming the utility of the MFB on fixing the total cost and avoiding any computational overhead if these parameters are not optimal.

## 7.2 Robustness with respect to the physical parameters

In this set of test examples, we want to show the robustness of the algorithms with respect to  $\alpha_\gamma$  and  $\beta$ . Note that  $\alpha_\gamma$  controls the strength of the fracture-matrix coupling, while  $\beta$  controls the strength of the non-linearity. We fix the mesh size  $h = 0.125$  and the time step  $\tau = 2^{-3}$ .

In Table 2 (top), we study the dependency of the number of iterations on the Forchheimer coefficient  $\beta$ . The LDD solvers show a weak dependency of the number of iterations on the values of  $\beta$ , giving slightly better results for larger values. Overall, the monolithic solver MoLDD performs slightly better than the iterative one ItLDD. Bear in mind that changing  $\beta$ , directly influences  $L_{\gamma,u}$ . This shows that this parameter should be optimized in accordance to the given value of  $\beta$ . Again, we suggest that the decrease in number of iterations over time steps may be due to using the previous iteration solution as the initial guess in the subsequent iteration. Clearly, we can conclude that the two solvers remain robust when strengthening the non-linearity effects. Moreover, all the simulations in Table 2 (top) are run with a fixed computational cost. The number of subdomain solves needed to carry out the simulations in Table 2 (top) is equal to 32 subdomain solves (Num. of DOF \* Num. of subdo. + 2 \*  $N$ ). Thus, strengthening or changing the non-linearity effects, for which maybe the number of iterations increases if the amount of stabilization via  $L_{\gamma,u}$  and/or  $L_{\gamma,p}$  is not carefully set, has no practical effects on the total computational costs. This gain in the computational resources which is in *conformity* with the spirit of *reduced basis* confirms that the MFB is an essential tool in the implementation of our LDD solvers.

Turning now to the effect of the fracture-matrix coupling on the two LDD solvers, we plot in Table 2 (bottom) the dependency of the number of iterations on the Robin parameter  $\alpha_\gamma$ . Clearly, the number of iterations remains stable when strengthening or weakening matrix-fracture coupling, confirming and concluding the robustness of both schemes with respect to  $\alpha_\gamma$ . Example of solution is reported in Figure 3. For the computational cost of the results in Table 2 (bottom), any change of  $\alpha_\gamma$  requires re-computing the

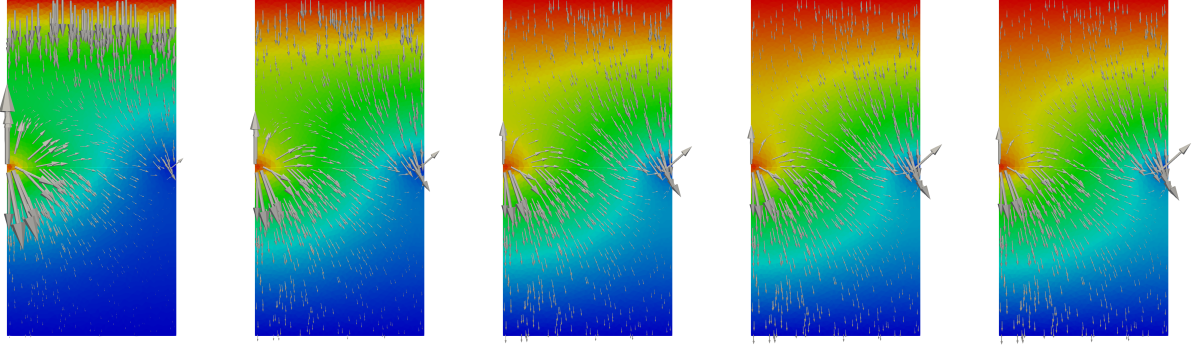


Figure 3:  $p \in [0, 1]$  and  $\mathbf{u}$  for the example in Subsection 7.2 with  $\beta = 10^2$  and  $\alpha_\gamma = 10^4$ .

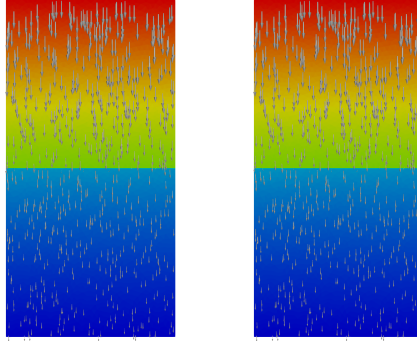


Figure 4:  $p \in [0, 1]$  and  $\mathbf{u}$  for the example in Subsection 7.3 with  $\mathbf{K}_\gamma = 10^{-4}\mathbf{I}$ ,  $\beta = 1$  and  $\alpha_\gamma = 1$ . With fine (left) and coarse (right) mortar grids.

multiscale flux basis. However, this cost remains fixed when running and comparing the two LDD solvers for a fixed  $\alpha_\gamma$ .

### 7.3 Flexibility of coarsening/refining the mortar grids

In this set of simulations, we consider the case of weak inter-dimensional coupling by fixing  $\alpha_\gamma = 1$ , with a low permeable fracture with  $\mathbf{K}_\gamma = 10^{-4}\mathbf{I}$ . We fix the following parameters:  $h = 2^{-5}$  (on the matrix),  $L_{\gamma,u} = 1$ ,  $L_{\gamma,p} = 2 \cdot 10^2$  and  $\beta = 1$ . We allow for a coarse scale of the mortar grids on the fracture;  $h_\gamma = 2^{-3}$ ,  $h_\gamma = 2^{-4}$ ,  $h_\gamma = 2^{-5}$ , where the last choice corresponds to matching grids on the fracture. In Table 3, we plot the resulting number of iterations required by each LDD solver. Particularly, we can see that the sequential ItLDD solver in the matching grids has more difficulty to converge, so the effectiveness of the MFB is more pronounced. The monolithic solver MoLDD seems to be more robust with refining the mortar grids. Here, the computational cost of the construction of the inter-dimensional operator benefits from fewer mortar degrees on the fracture. Example of a solution is depicted in Figure 4, where we can see that conforming and non-conforming gridding (with  $h_\gamma = 2^{-3}$ ) on the fracture give indistinguishable results.

### 7.4 Extension to other flow models: the Cross model

The aim of this test case is to show that our LDD solvers can be applied to more general flow models. On the fracture, we assume the Cross flow model to relate  $p_\gamma$  and  $\mathbf{u}_\gamma$ . We have the non-linear term given by

$$\xi(\mathbf{u}_\gamma) = \frac{(\omega_0 - \omega_\infty)\mathbf{u}_\gamma}{1 + K_\gamma|\mathbf{u}_\gamma|^{2-r}}.$$



$\# \text{cells} \backslash n$	1	2	3	4	5
8	3	3	3	3	2
16	3	3	3	3	2
64	3	3	3	3	2

$\# \text{cells} \backslash n$	1	2	3	4	5
8	11	10	10	9	9
16	11	10	10	9	9
64	18	15	15	15	14

Table 3: Results for the example of Subsection 7.3 reporting the number of iterations for conforming and non-conforming (coarse scale) grids on the fracture. Left table corresponds to solving with the MoLDD scheme, while the right one corresponds to solving with the ItLDD scheme.

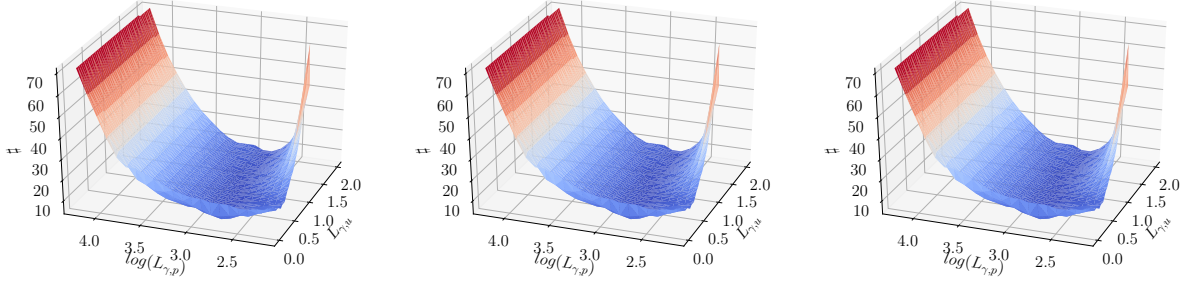


Figure 5: Results for the example of Subsection 7.4 using ItLDD scheme. We report the number of iterations  $\#$  for different values of  $L_{\gamma,u}$  and  $L_{\gamma,p}$ . On the left for the first time step, in the centre for the third, and on the right for the last time step.

The parameters  $0 \leq \omega_\infty < \omega_0$ ,  $\zeta$  and  $r$  are positive scalars related to the rheology of the considered liquid. In (1.2a),  $\mathbf{K}_\gamma$  is now replaced by  $\omega_\infty$ . We let  $\omega := \omega_\infty - \omega_0$  and set  $\omega_0 = 2$ ,  $\omega_\infty = 1$ ,  $\zeta = 1$ , and  $r = 1.5$ . It is easy to verify that  $\xi$  satisfies the assumption (A1). For more details see [24, 25] and the references therein.

We choose the iterative solver ItLDD and re-compute the simulations of Subsection 7.1 and 7.2 for the Cross flow model. We set then  $L_{\gamma,u} = L_\xi/2 = 0.5$  and  $L_{\gamma,p} = \alpha_\gamma = 10^3$  as derived from the theory. The results (not shown) demonstrate first the stability of the ItLDD solver with respect to the parameters  $h$  and  $\tau$ . Crucially, all the simulations in this example do not require additional computational cost (except fracture solves), as we use the same MFB inherited from the Forchheimer model. We set  $h = 2^{-5}$  with slightly coarse grids on the fracture  $h_\gamma = 2^{-4}$  and  $\tau = 2^{-4}$ .

In Figure 5, we show the results for the ItLDD solver on a set of realizations of  $(L_{\gamma,u}, L_{\gamma,p})$ . The results do not differ greatly comparing to the case of Forchheimer's flow model. The convexity of the surface plots in all time steps is clear giving away an optimal combination of values for  $L_{\gamma,u}$  and  $L_{\gamma,p}$ . For example, we can find minimum of 5 iterations for  $L_{\gamma,u}$  between approximately 0.73 and 1.57, and  $L_{\gamma,p}$  between  $10^{2.8}$  and  $10^3$ . Note that the parameters prescribed by the theoretical results,  $L_{\gamma,u} = 0.5$  and  $L_{\gamma,p} = 10^3$ , form a good candidate in this simulation. Finally, we mention that we can use an optimization process, as detailed in [50], in order to get the optimal values. Precisely, the fact that the choice of the stabilization parameters is independent of the mesh size, one can then run the LDD solver on a coarse spatial mesh and one time step, and study the stabilization parameters in specific intervals centred around the theoretical values. The parameters that give the lowest number of iterations are then used for the real computations. This “brute-force” optimization is simple to do in practice when using the MFB.

In Table 4, we consider to test the dependency of the number of iterations on the rheology parameters of

$\omega \backslash n$	1	2	3	4	5
0.1	15	11	10	9	8
1	10	9	8	8	8
2.5	30	19	16	14	12

$\zeta \backslash n$	1	2	3	4	5
1	10	9	8	8	7
10	11	9	9	8	7
100	16	11	10	9	8

$r \backslash n$	1	2	3	4	5
1	10	9	9	8	7
1.5	10	9	8	8	7
4.5	17	11	10	9	8

Table 4: Results for the example of Subsection 7.4. On the left the number of iterations by varying the values of  $\omega$ . In the center when  $\zeta$  changes, while on the right for different values of  $r$ .

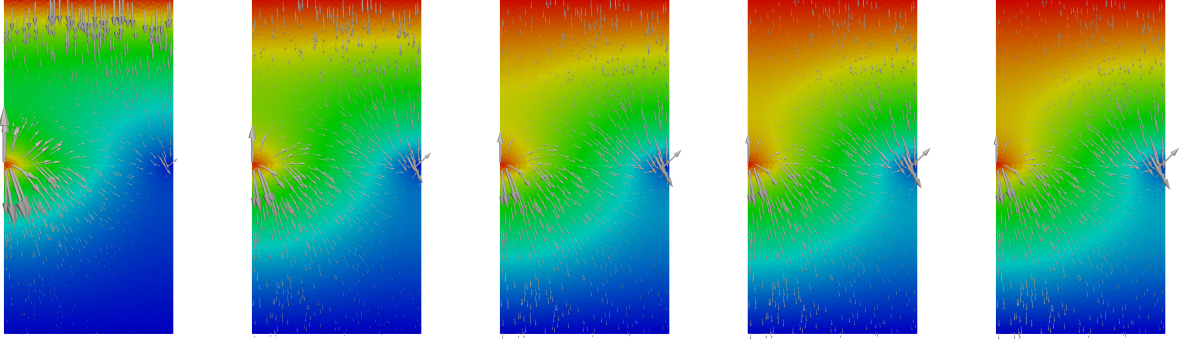


Figure 6:  $p \in [0, 1]$  and  $\mathbf{u}$  for the example in Subsection 7.4 with  $\omega = 1$ ,  $\zeta = 1$ , and  $r = 1.5$ .

the flow model. We provide results of several tests on  $\omega$ ,  $\zeta$ , and  $r$ . While testing for one of the parameters, the other two are fixed to either  $\omega = 1$ ,  $\zeta = 1$  or  $r = 1.5$ . We can observe that  $\omega$  strongly influences the performance of both methods making it difficult to converge when  $\omega$  gets larger, that is, when the non-linearity is stronger. For larger values of  $\omega$  the number of iterations increases drastically, suggesting the necessity to adjust the  $L$ -scheme parameters as well as to use the MFB. The number of iterations was less dependent of the parameter  $\zeta$ . This parameter itself contributes less to the strength of the non-linearity in comparison to  $\omega$ , and, thus, influencing less the performance of the solver. Finally, we can again notice a moderate dependency of number of iterations on parameter  $r$ . This is especially shown when  $r > 2$  and the exponent on the vector norm of  $\mathbf{u}_\gamma$  becomes negative. Thus, the non-linear flow function  $\xi$  is exponential in the values of  $\mathbf{u}_\gamma$  and accounts for the very fast flow in the fractures. We finally recall that the robustness study drawn in Table 4 has the cost of one realization with fixed-parameters, confirming the role of the MFB in our solvers. For the robustness of LDD solvers with respect to the matrix-fracture coupling effects induced by the parameter  $\alpha_\gamma$ , we have seen that both solvers are robust when strengthening or weakening the coupling effects (results not shown). Example of solution is reported in Figure 6.

## 8 Conclusions

In this study, we have presented two new strategies to solve a compressible single-phase flow problem in a porous medium with a fracture. In the porous medium, we have considered the classical Darcy relation between the velocity and the pressure while, in the fracture, a general non-linear law. We employ the  $L$ -scheme to handle the non-linearity term, but also to treat the inter-dimensional coupling in the second proposed algorithm. To further achieve computational speed-up, the linear Robin-to-Neumann co-dimensional map is constructed in an offline phase resulting in a problem reduced only to the fracture interface. This approach allows to change the fracture parameters, or the fracture flow model in general, without the need to recompute the problem associated with the rock matrix. We have shown the existence of optimal values for the  $L$ -scheme parameters, which are validated through several numerical tests. Future developments can be explored towards domain decomposition in time, where fast and slow fractures are solved asynchronously.

## Acknowledgements

We acknowledge the financial support from the Research Council of Norway for the TheMSES project (project no. 250223) and the ANIGMA project (project no. 244129/E20) through the ENERGIX program.

## References

- [1] E. AHMED, A. FUMAGALLI, AND A. BUDIŠA, *A multiscale flux basis for mortar mixed discretizations of reduced darcy-forchheimer fracture models*, Computer Methods in Applied Mechanics and Engineering,

- (2019), <https://doi.org/https://doi.org/10.1016/j.cma.2019.05.034>.
- [2] E. AHMED, S. A. HASSAN, C. JAPHET, M. KERN, AND M. VOHRALÍK, *A posteriori error estimates and stopping criteria for space-time domain decomposition for two-phase flow between different rock types*, working paper or preprint, June 2017, <https://hal.inria.fr/hal-01540956>.
  - [3] E. AHMED, J. JAFFRÉ, AND J. E. ROBERTS, *A reduced fracture model for two-phase flow with different rock types*, Math. Comput. Simulation, 137 (2017), pp. 49–70, <https://doi.org/10.1016/j.matcom.2016.10.005>.
  - [4] E. AHMED, J. M. NORDBOTTEN, AND F. A. RADU, *Adaptive asynchronous time-stepping, stopping criteria, and a posteriori error estimates for fixed-stress iterative schemes for coupled poromechanics problems*, arXiv:1901.01206 [math.NA], (2019), <https://arxiv.org/abs/1901.01206>.
  - [5] C. ALBOIN, J. JAFFRÉ, J. E. ROBERTS, AND C. SERRES, *Modeling fractures as interfaces for flow and transport in porous media*, in Fluid flow and transport in porous media: mathematical and numerical treatment (South Hadley, MA, 2001), vol. 295 of Contemp. Math., Amer. Math. Soc., Providence, RI, 2002, pp. 13–24, <https://doi.org/10.1090/conm/295/04999>.
  - [6] P. ANGOT, F. BOYER, AND F. HUBERT, *Asymptotic and numerical modelling of flows in fractured porous media*, M2AN Math. Model. Numer. Anal., 43 (2009), pp. 239–275, <https://doi.org/10.1051/m2an/2008052>.
  - [7] P. F. ANTONIETTI, J. DE PONTI, L. FORMAGGIA, AND A. SCOTTI, *Preconditioning techniques for the numerical solution of flow in fractured porous media*, MOX Report 17, Politecnico di Milano, 2019.
  - [8] P. F. ANTONIETTI, L. FORMAGGIA, A. SCOTTI, M. VERANI, AND N. VERZOTT, *Mimetic finite difference approximation of flows in fractured porous media*, ESAIM Math. Model. Numer. Anal., 50 (2016), pp. 809–832, <https://doi.org/10.1051/m2an/2015087>.
  - [9] T. ARBOGAST, G. PENCHEVA, M. F. WHEELER, AND I. YOTOV, *A multiscale mortar mixed finite element method*, Multiscale Model. Simul., 6 (2007), pp. 319–346, <https://doi.org/10.1137/060662587>.
  - [10] M. ARSHAD, E.-J. PARK, AND D.-W. SHIN, *Analysis of multiscale mortar mixed approximation of nonlinear elliptic equations*, Comput. Math. Appl., 75 (2018), pp. 401–418, <https://doi.org/10.1016/j.camwa.2017.09.031>.
  - [11] A. BENACEUR, V. EHRLACHER, A. ERN, AND S. MEUNIER, *A progressive reduced basis/empirical interpolation method for nonlinear parabolic problems*, SIAM J. Sci. Comput., 40 (2018), pp. A2930–A2955, <https://doi.org/10.1137/17M1149638>.
  - [12] H. BERNINGER, S. LOISEL, AND O. SANDER, *The 2-Lagrange multiplier method applied to nonlinear transmission problems for the Richards equation in heterogeneous soil with cross points*, SIAM J. Sci. Comput., 36 (2014), pp. A2166–A2198, <https://doi.org/10.1137/120901064>, <https://doi.org/10.1137/120901064>.
  - [13] I. BERRE, F. DOSTER, AND E. KEILEGAVLEN, *Flow in fractured porous media: A review of conceptual models and discretization approaches*, Transport in Porous Media, (2018), <https://doi.org/10.1007/s11242-018-1171-6>.
  - [14] W. M. BOON, J. M. NORDBOTTEN, AND I. YOTOV, *Robust discretization of flow in fractured porous media*, SIAM J. Numer. Anal., 56 (2018), pp. 2203–2233, <https://doi.org/10.1137/17M1139102>.
  - [15] M. BORREGALES, F. A. RADU, K. KUMAR, AND J. M. NORDBOTTEN, *Robust iterative schemes for non-linear poromechanics*, Comput. Geosci., 22 (2018), pp. 1021–1038, <https://doi.org/10.1007/s10596-018-9736-6>.
  - [16] K. BRENNER, J. HENNICKER, R. MASSON, AND P. SAMIER, *Hybrid-dimensional modelling of two-phase flow through fractured porous media with enhanced matrix fracture transmission conditions*, J. Comput. Phys., 357 (2018), pp. 100–124, <https://doi.org/10.1016/j.jcp.2017.12.003>.

- [17] M. K. BRUN, E. AHMED, I. BERRE, J. M. NORDBOTTEN, AND F. A. RADU, *Monolithic and splitting based solution schemes for fully coupled quasi-static thermo-poroelasticity with nonlinear convective transport*, arXiv:1902.05783 [math.NA], (2019), <https://arxiv.org/abs/1902.05783>.
- [18] A. BUDIŠA AND X. HU, *Block preconditioners for mixed-dimensional discretization of flow in fractured porous media*, arXiv:1905.13513 [math.NA], (2019), <https://arxiv.org/abs/1905.13513>.
- [19] S. CHEN AND H. RUI, *A two-grid decoupled algorithm for fracture models*, Comput. Math. Appl., 76 (2018), pp. 1161–1173, <https://doi.org/10.1016/j.camwa.2018.06.005>.
- [20] C. D'ANGELO AND A. SCOTTI, *A mixed finite element method for Darcy flow in fractured porous media with non-matching grids*, Mathematical Modelling and Numerical Analysis, 46 (2012), pp. 465–489, <https://doi.org/10.1051/m2an/2011148>.
- [21] M. DEL PRA, A. FUMAGALLI, AND A. SCOTTI, *Well posedness of fully coupled fracture/bulk Darcy flow with XFEM*, SIAM J. Numer. Anal., 55 (2017), pp. 785–811, <https://doi.org/10.1137/15M1022574>.
- [22] V. DOLEAN, P. JOLIVET, AND F. NATAF, *An introduction to domain decomposition methods*, Society for Industrial and Applied Mathematics (SIAM), Philadelphia, PA, 2015, pp. x+238, <https://doi.org/10.1137/1.9781611974065.ch1>. Algorithms, theory, and parallel implementation.
- [23] A. ERN AND J.-L. GUERMOND, *Evaluation of the condition number in linear systems arising in finite element approximations*, M2AN Math. Model. Numer. Anal., 40 (2006), pp. 29–48, <https://doi.org/10.1051/m2an:2006006>.
- [24] V. J. ERVIN, E. W. JENKINS, AND S. SUN, *Coupling nonlinear Stokes and Darcy flow using mortar finite elements*, Appl. Numer. Math., 61 (2011), pp. 1198–1222, <https://doi.org/10.1016/j.apnum.2011.08.002>.
- [25] V. J. ERVIN, H. LEE, AND A. J. SALGADO, *Generalized Newtonian fluid flow through a porous medium*, J. Math. Anal. Appl., 433 (2016), pp. 603–621, <https://doi.org/10.1016/j.jmaa.2015.07.054>.
- [26] L. FORMAGGIA, A. FUMAGALLI, A. SCOTTI, AND P. RUFFO, *A reduced model for Darcy's problem in networks of fractures*, ESAIM Math. Model. Numer. Anal., 48 (2014), pp. 1089–1116, <https://doi.org/10.1051/m2an/2013132>.
- [27] N. FRIH, V. MARTIN, J. E. ROBERTS, AND A. SAÂDA, *Modeling fractures as interfaces with non-matching grids*, Computational Geosciences, 16 (2012), pp. 1043–1060, <https://doi.org/10.1007/s10596-012-9302-6>.
- [28] N. FRIH, J. E. ROBERTS, AND A. SAADA, *Modeling fractures as interfaces: a model for Forchheimer fractures*, Comput. Geosci., 12 (2008), pp. 91–104, <https://doi.org/10.1007/s10596-007-9062-x>.
- [29] A. FUMAGALLI AND A. SCOTTI, *A reduced model for flow and transport in fractured porous media with non-matching grids*, in Numerical Mathematics and Advanced Applications 2011, A. Cangiani, R. L. Davidchack, E. Georgoulis, A. N. Gorban, J. Levesley, and M. V. Tretyakov, eds., Berlin, Heidelberg, 2013, Springer Berlin Heidelberg, pp. 499–507, [https://doi.org/10.1007/978-3-642-33134-3\\_53](https://doi.org/10.1007/978-3-642-33134-3_53).
- [30] B. GANIS, G. PENCHEVA, M. F. WHEELER, T. WILDEY, AND I. YOTOV, *A frozen Jacobian multiscale mortar preconditioner for nonlinear interface operators*, Multiscale Model. Simul., 10 (2012), pp. 853–873, <https://doi.org/10.1137/110826643>.
- [31] B. GANIS, D. VASSILEV, C. WANG, AND I. YOTOV, *A multiscale flux basis for mortar mixed discretizations of Stokes-Darcy flows*, Comput. Methods Appl. Mech. Engrg., 313 (2017), pp. 259–278, <https://doi.org/10.1016/j.cma.2016.09.037>.
- [32] B. GANIS AND I. YOTOV, *Implementation of a mortar mixed finite element method using a multiscale flux basis*, Comput. Methods Appl. Mech. Engrg., 198 (2009), pp. 3989–3998, <https://doi.org/10.1016/j.cma.2009.09.009>.

- [33] V. GIRAULT AND M. F. WHEELER, *Numerical discretization of a Darcy-Forchheimer model*, Numer. Math., 110 (2008), pp. 161–198, <https://doi.org/10.1007/s00211-008-0157-7>.
- [34] H. HÆGLAND, A. ASSTEERAWATT, H. DAHLE, G. EIGESTAD, AND R. HELMIG, *Comparison of cell- and vertex-centered discretization methods for flow in a two-dimensional discrete-fracture-matrix system*, Advances in Water Resources, 32 (2009), pp. 1740–1755, <https://doi.org/10.1016/j.advwatres.2009.09.006>.
- [35] T.-T.-P. HOANG, C. JAPHET, M. KERN, AND J. E. ROBERTS, *Space-time domain decomposition for reduced fracture models in mixed formulation*, SIAM J. Numer. Anal., 54 (2016), pp. 288–316, <https://doi.org/10.1137/15M1009651>.
- [36] E. KEILEGAVLEN, A. FUMAGALLI, R. BERGE, I. STEFANSSON, AND I. BERRE, *Porepy: An open source simulation tool for flow and transport in deformable fractured rocks*, tech. report, arXiv:1712.00460 [cs.CE], 2017, <https://arxiv.org/abs/1712.00460>.
- [37] M.-Y. KIM AND E.-J. PARK, *Fully discrete mixed finite element approximations for non-Darcy flows in porous media*, Comput. Math. Appl., 38 (1999), pp. 113–129, [https://doi.org/10.1016/S0898-1221\(99\)00291-6](https://doi.org/10.1016/S0898-1221(99)00291-6).
- [38] P. KNABNER AND J. E. ROBERTS, *Mathematical analysis of a discrete fracture model coupling Darcy flow in the matrix with Darcy-Forchheimer flow in the fracture*, ESAIM Math. Model. Numer. Anal., 48 (2014), pp. 1451–1472, <https://doi.org/10.1051/m2an/2014003>.
- [39] M. LESINIGO, C. D’ANGELO, AND A. QUARTERONI, *A multiscale Darcy-Brinkman model for fluid flow in fractured porous media*, Numer. Math., 117 (2011), pp. 717–752, <https://doi.org/10.1007/s00211-010-0343-2>.
- [40] F. LIST, K. KUMAR, I. S. POP, AND F. A. RADU, *Upscaling of unsaturated flow in fractured porous media*, arXiv preprint arXiv:1807.05993, (2018).
- [41] F. LIST AND F. A. RADU, *A study on iterative methods for solving Richards’ equation*, Comput. Geosci., 20 (2016), pp. 341–353, <https://doi.org/10.1007/s10596-016-9566-3>.
- [42] W. LIU AND Z. SUN, *A block-centered finite difference method for reduced fracture model in Karst aquifer system*, Comput. Math. Appl., 74 (2017), pp. 1455–1470, <https://doi.org/10.1016/j.camwa.2017.06.028>.
- [43] V. MARTIN, J. JAFFRÉ, AND J. E. ROBERTS, *Modeling Fractures and Barriers as Interfaces for Flow in Porous Media*, SIAM J. Sci. Comput., 26 (2005), pp. 1667–1691, <https://doi.org/10.1137/S1064827503429363>.
- [44] K. MITRA AND I. POP, *A modified l-scheme to solve nonlinear diffusion problems*, Computers & Mathematics with Applications, 77 (2019), pp. 1722 – 1738, <https://doi.org/https://doi.org/10.1016/j.camwa.2018.09.042>. 7th International Conference on Advanced Computational Methods in Engineering (ACOMEN 2017).
- [45] J. M. NORDBOTTEN AND P. E. BJØRSTAD, *On the relationship between the multiscale finite-volume method and domain decomposition preconditioners*, Comput. Geosci., 12 (2008), pp. 367–376, <https://doi.org/10.1007/s10596-007-9066-6>, <https://doi.org/10.1007/s10596-007-9066-6>.
- [46] I. S. POP, F. RADU, AND P. KNABNER, *Mixed finite elements for the Richards’ equation: linearization procedure*, J. Comput. Appl. Math., 168 (2004), pp. 365–373, <https://doi.org/10.1016/j.cam.2003.04.008>.
- [47] A. QUARTERONI AND A. VALLI, *Domain decomposition methods for partial differential equations*, Numerical Mathematics and Scientific Computation, The Clarendon Press, Oxford University Press, New York, 1999. Oxford Science Publications.

- [48] N. SCHWENCK, B. FLEMISCH, R. HELMIG, AND B. I. WOHLMUTH, *Dimensionally reduced flow models in fractured porous media: crossings and boundaries*, Comput. Geosci., 19 (2015), pp. 1219–1230, <https://doi.org/10.1007/s10596-015-9536-1>.
- [49] D. SEUS, K. MITRA, I. S. POP, F. A. RADU, AND C. ROHDE, *A linear domain decomposition method for partially saturated flow in porous media*, Comput. Methods Appl. Mech. Engrg., 333 (2018), pp. 331–355, <https://doi.org/10.1016/j.cma.2018.01.029>.
- [50] E. STORVIK, J. W. BOTH, K. KUMAR, J. M. NORDBOTTEN, AND F. A. RADU, *On the optimization of the fixed-stress splitting for biot's equations*, International Journal for Numerical Methods in Engineering, (2019), <https://doi.org/10.1002/nme.6130>.
- [51] S. G. THOMAS AND M. F. WHEELER, *Enhanced velocity mixed finite element methods for modeling coupled flow and transport on non-matching multiblock grids*, Comput. Geosci., 15 (2011), pp. 605–625, <https://doi.org/10.1007/s10596-011-9227-5>.
- [52] K. URBAN AND B. WIELAND, *Affine decompositions of parametric stochastic processes for application within reduced basis methods*, IFAC Proceedings Volumes, 45 (2012), pp. 716–721, <https://doi.org/10.3182/20120215-3-AT-3016.00127>. 7th Vienna International Conference on Mathematical Modelling.
- [53] A. VENEZIANI, *Certified reduced basis methods for parametrized partial differential equations*, SIAM Rev., 59 (2017), pp. 219–221.
- [54] F. XING, R. MASSON, AND S. LOPEZ, *Parallel vertex approximate gradient discretization of hybrid dimensional Darcy flow and transport in discrete fracture networks*, Comput. Geosci., 21 (2017), pp. 595–617, <https://doi.org/10.1007/s10596-016-9606-z>.
- [55] Y. YANG, E. T. CHUNG, AND S. FU, *An enriched multiscale mortar space for high contrast flow problems*, Commun. Comput. Phys., 23 (2018), pp. 476–499, <https://doi.org/10.4208/cicp.OA-2016-0147>.